

## Capped Subporphyrins

Yasuhide Inokuma and Atsuhiko Osuka\*<sup>[a]</sup>

**Abstract:** Capped subporphyrins **12–16** with  $C_3$  molecular symmetry were synthesized from 5,10,15-tri(3-aminophenyl)-substituted subporphyrin **8** and tripodal trialdehydes **2–6** by Lindsey's entropically favored macrocyclization. X-ray diffraction analysis has revealed that the concave surface of the subporphyrin core is selectively capped with a 1,3,5-substituted benzene moiety. Capped subporphyrins **15** and **16**, with a five-atom arm and thus large inner cavities, exhibit solvent incorporation behavior in their crystal structures. On the other hand, subporphyrins **12** and

**13** exhibit tight structures, in which the cap and subporphyrin core are found much closer with average interplanar separations of 3.56 and 3.15 Å, respectively. Variable-temperature  $^1\text{H}$  NMR measurements revealed that subporphyrins **12**, **13**, and **16** undergo spiral interconversions between *P* and *M* forms depending on the arm length and the electronic nature of the cap.

**Keywords:** cage compounds • porphyrinoids • spiral interconversions • substituent effects

Of these, subporphyrin **13**, with a 1,3,5-tri(alkoxycarbonyl)benzene cap strapped by three-atom arms, exhibits a considerably slow spiral interconversion with a large enthalpy change of  $\Delta H^\ddagger = 76.4 \text{ kJ mol}^{-1}$  and a characteristic redshift of the Soret-like band and enhancement of the Q(0,0) band. These properties are ascribed to considerable through-space charge-transfer interactions between the electron-deficient cap and the subporphyrin core and the multiple CH– $\pi$  interactions.

### Introduction

The chemistry of subporphyrin, which is a genuine contracted porphyrin with a  $14\pi$ -aromatic macrocycle, began with our discovery of tribenzosubporphines in 2006.<sup>[1]</sup> The following years have witnessed the exploration of an increasing number of subporphyrins and their related compounds with rich optical, electrochemical, and structural properties.<sup>[2–9]</sup> Among them, *meso*-aryl-substituted subporphyrins<sup>[4]</sup> have been found to be particularly interesting in light of their highly tunable optical and electrochemical properties by large *meso*-aryl substituents. These features mainly arise from free rotation of the 2,6-unsubstituted aryl substituents at *meso* positions, which allow effective conjugative interactions between the *meso*-aryl groups and the subporphyrin. Similarly, various functional groups have been introduced to

the *meso* positions of subporphyrin to tune the electronic properties of the subporphyrins.<sup>[4–7]</sup> For example, elongation of the  $\pi$ -electronic network by substitution of oligo(*p*-phenyleneethynylene) arms resulted in the intensification and redshift of the Soret-like band and the enhancements in both the fluorescence quantum yield and the two-photon absorption (TPA) cross section.<sup>[5]</sup> Substitution with the 4-(*N,N*-dialkylamino)phenyl group caused strong intramolecular charge-transfer interactions, which gave substantial perturbation on the absorption and fluorescence spectra of subporphyrin.<sup>[6]</sup> Considerable through-bond interactions between two subporphyrin cores were observed for the 4,4'-biphenylene-bridged dimer in the ground state, but not for the 3,3'-homologue.<sup>[7]</sup> On the other hand, chemical modulations at the  $\beta$  positions provide large electronic impacts on the subporphyrin macrocycle. Hence, hydrogenation of one  $\beta$ = $\beta$  double bond of subporphyrin yielded *meso*-aryl subchlorin, which displays a blueshifted and broadened Soret-like band and redshifted and intensified Q-like bands.<sup>[8]</sup> A hexabromination–Stille coupling strategy provided hexaethynylated subporphyrins in high yields, which exhibited large TPA cross sections up to 2800 GM.<sup>[9]</sup> Importantly, most of these attractive properties are very difficult or almost impossible for porphyrins in which peripheral substituents are arranged in an almost orthogonal manner.

[a] Dr. Y. Inokuma, Prof. Dr. A. Osuka  
Department of Chemistry, Graduate School of Science  
Kyoto University, Sakyo-ku, Kyoto 6068502 (Japan)  
Fax: (+81) 75-753-3970  
E-mail: osuka@kuchem.kyoto-u.ac.jp

Supporting information for this article is available on the WWW under <http://dx.doi.org/10.1002/chem.200900879>.

Subporphyrins adopt a bowl-shaped triangular structure, which is common for subphthalocyanines.<sup>[10]</sup> Recently, such bowl-shaped  $\pi$ -conjugated systems have attracted increasing attention in light of curved aromatic systems, unique recognition abilities, and partial structural components of fullerenes and carbon nanotubes.<sup>[11]</sup> Whereas the representative bowl-shaped aromatic hydrocarbon systems, such as sumanenes and corranulenes, are known to undergo bowl-to-bowl flipping,<sup>[12]</sup> none such dynamic motions have been observed for subporphyrins or subphthalocyanines, which suggests their structural robustness. We thought that this structural feature of subporphyrins should be advantageous for fabrication at the concave face, whereas such a face-selective fabrication has been quite rare both for subporphyrins and subphthalocyanines. Rare examples include 1) a chirally discriminating assembly of subphthalocyanines, which was reported to provide a dimeric cage with linkages at the concave face<sup>[13]</sup> and 2) a boron axial-ligand exchange reaction used to construct complementary face-to-face subporphyrin dimers with linkages at the convex face.<sup>[14]</sup>

Herein, we report the synthesis and characterization of capped subporphyrins in which a 1,3,5-trisubstituted benzene cap is connected to a subporphyrin core at the concave side. Whereas there are many examples of capped porphyrins in the literature,<sup>[14–16]</sup> there are no such precedents for subporphyrin. It can be expected for capped subporphyrins that 1) intramolecular through-space  $\pi$ – $\pi$  interactions between the concave face and the 1,3,5-trisubstituted cap is possible, 2) a guest molecule of a suitable size and shape can be encapsulated into a cavity created by the subporphyrin core and cap, and 3) such a subporphyrin cap restricts free rotation of the *meso*-aryl substituents, hence influencing the electronic interaction of the subporphyrin core with the *meso*-aryl substituents. During this work, we confirmed all of these expectations and additionally found that spiral interconversions of capped subporphyrins depend upon the length of bridges that connect the subporphyrin core and cap and upon the electronic nature of the cap.

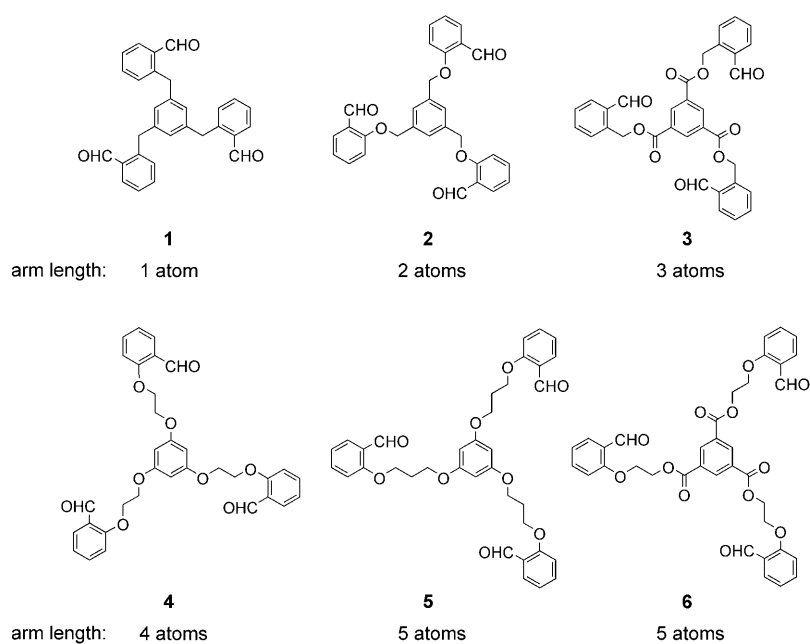
## Results and Discussion

**Synthesis:** There are two synthetic approaches to capped porphyrins: One is the direct synthesis of a porphyrin macrocycle from pyrrole and a covalently linked tetraaldehyde.<sup>[15]</sup> The other is a stepwise synthesis that consists of the initial porphyrin synthesis and subsequent capping with quadruple

linkage.<sup>[16,17]</sup> First, we attempted the direct method for the synthesis of capped subporphyrins. To preserve  $C_3$  molecular symmetry of the subporphyrin core, 1,3,5-trisubstituted benzene moiety was employed as a cap model. Scheme 1 shows tripodal aryl aldehydes **1–6** used for the direct synthesis. The arm length is defined by the number of atoms between the central benzene moiety and the peripheral benzaldehyde unit; this is also indicated in Scheme 1.

An equimolar mixture of pyridine-tri-*N*-pyrrolylborane (**7**) and a tripodal aryl aldehyde was treated with trifluoroacetic acid (TFA) in 1,2-dichlorobenzene at 0°C. After the acid catalyst was quenched with pyridine, the solution was heated at reflux under aerobic conditions. However, this standard reaction for *meso*-aryl-substituted subporphyrins did not yield capped subporphyrin. Therefore, we examined the stepwise approach. One of the most efficient stepwise synthetic protocols of capped porphyrin was developed by Lindsey and Mauzerall, who employed entropically controlled macrocyclization between the  $\alpha,\alpha,\alpha,\alpha$ -atropisomer of *meso*-tetrakis(2-aminophenyl)porphyrin and a tetraaldehyde.<sup>[17]</sup> As such, the stereocontrolled  $\alpha,\alpha,\alpha,\alpha$ -atropisomer was required for the synthesis of capped porphyrins because of restricted rotation of the *meso*-aryl substituents in porphyrins. It was thought, however, that such a care would not be obligatory in the application of this strategy to subporphyrins owing to free rotation of the *meso*-aryl substituents. We thus examined a similar macrocyclization reaction for *meso*-tri(3-aminophenyl)-substituted subporphyrin **8** and tripodal aldehydes **1–6**.

Subporphyrin **8** was first synthesized from *meso*-tri(3-nitrophenyl)-substituted subporphyrin **9** by means of an  $\text{SnCl}_2 \cdot 2\text{H}_2\text{O}$  reduction in a mixture of EtOH and hydrochloric acid. Although the reduction of three nitro groups of **9**

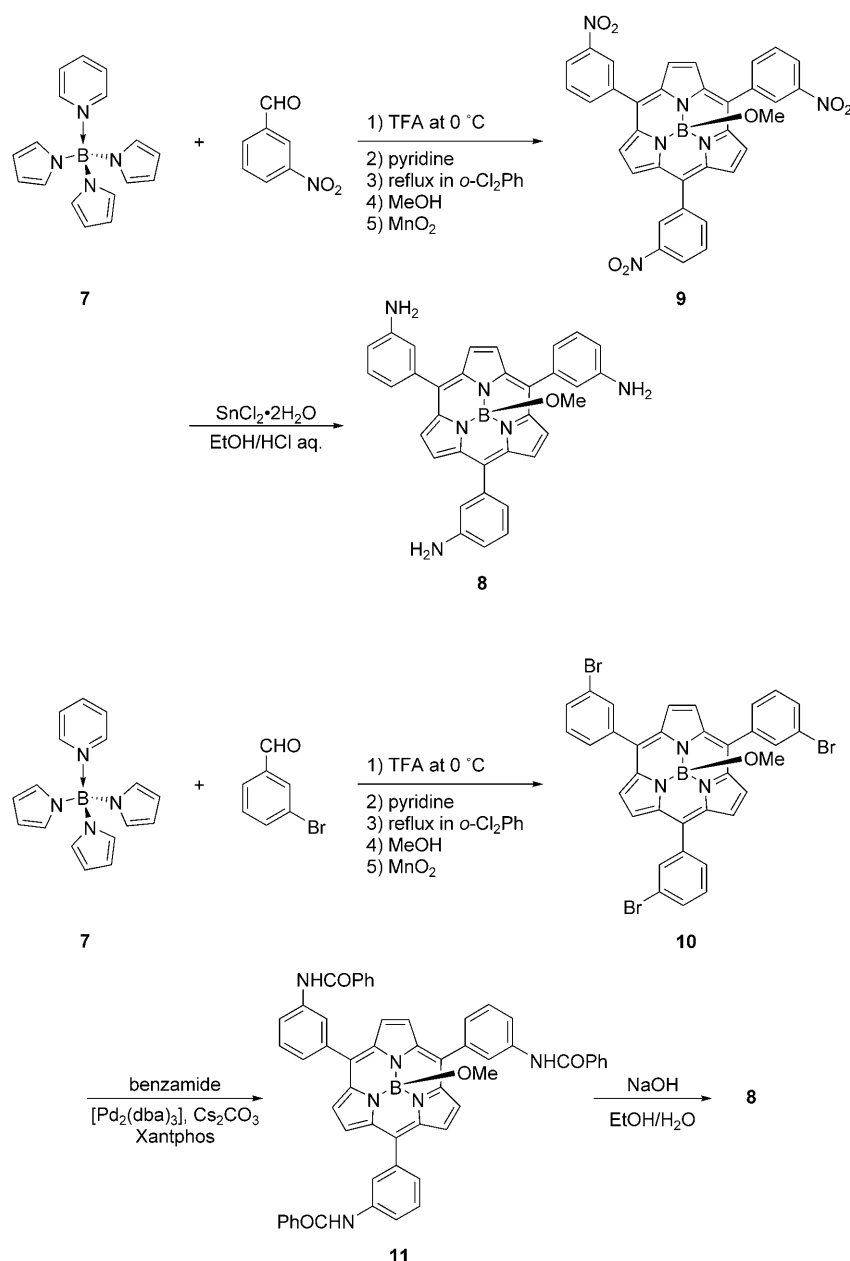


Scheme 1. Structures of tripodal aryl aldehydes **1–6**. The arm lengths are also indicated.

proceeded quantitatively, the very poor yield of **9** (less than 1%) posed a serious obstacle for further investigation. As an alternative route, *meso*-tris(3-bromophenyl)-substituted subporphyrin **10** was prepared from **7** and 3-bromobenzaldehyde in 4.9% yield under the standard conditions.<sup>[4c]</sup> Subporphyrin **10** was coupled with benzamide in the presence of  $[\text{Pd}_2(\text{dba})_3]$ ,  $\text{Cs}_2\text{CO}_3$ , and Xantphos under the reaction conditions reported by Yin and Buchwald to furnish *meso*-tris(3-benzamidophenyl)-substituted subporphyrin **11** in 82% yield.<sup>[18]</sup> The amido groups in **11** were readily hydrolyzed with NaOH in a mixture of EtOH/THF/water to give subporphyrin **8** in 92% yield. Hence, the overall yield of **8** from **7** was 3.7% yield over 3 steps (Scheme 2). The  $^1\text{H}$  NMR spectrum of subporphyrin **8** in  $\text{CDCl}_3$  exhibits a

sharp singlet at  $\delta=8.13$  ppm due to the six  $\beta$  protons and a single set of signals due to the 3-aminophenyl groups (a singlet at  $\delta=7.41$  ppm, two doublets at  $\delta=7.40$  and 6.92 ppm, and a triplet at  $\delta=7.45$  ppm), indicating free rotation of *meso*-3-aminophenyl substituents in solution.

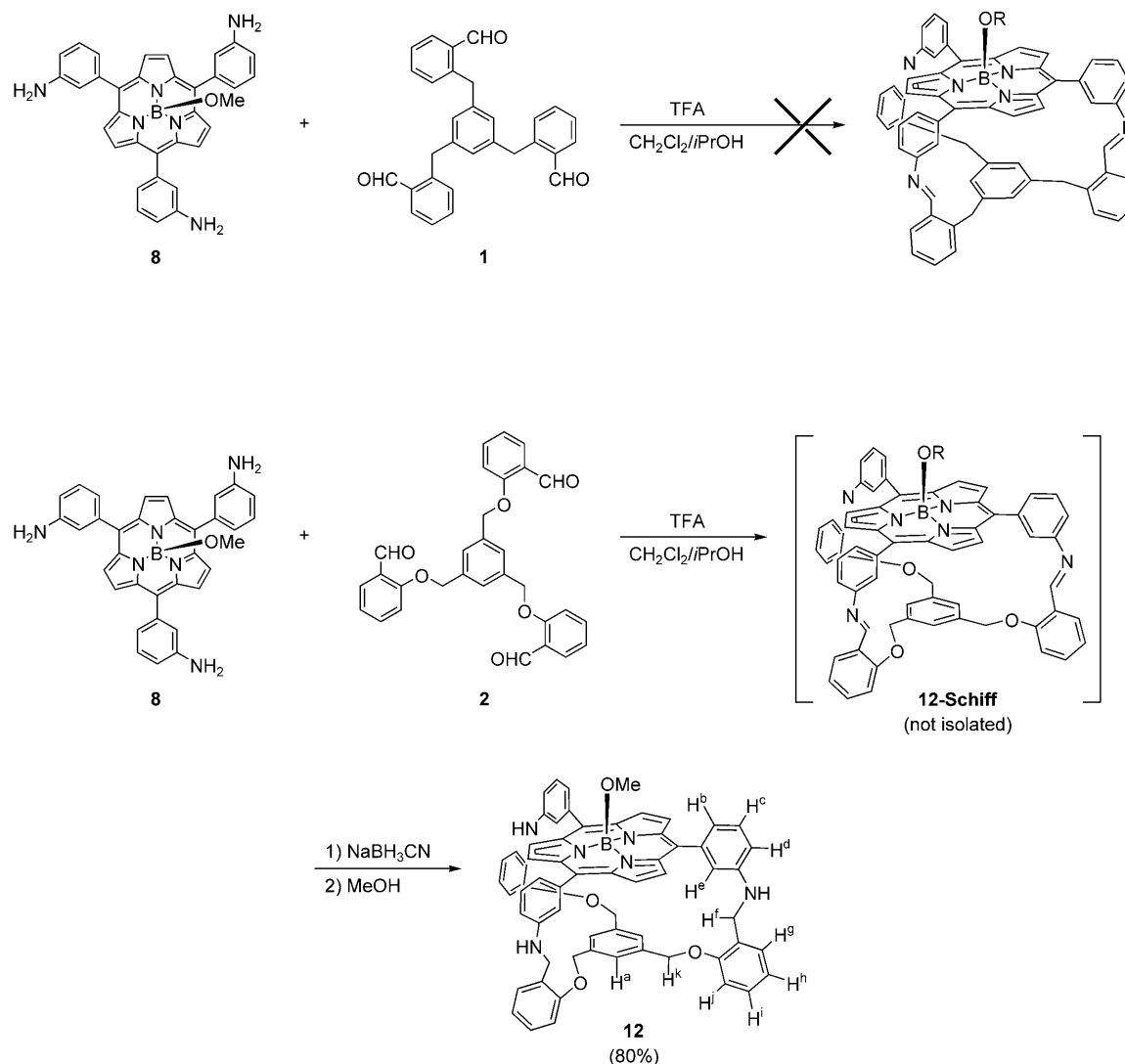
The stepwise capping reaction was first examined for **8** and trialdehyde **1**. These two components were condensed under various reaction conditions in the presence of an acid catalyst. However, the  $^1\text{H}$  NMR spectrum of the reaction products showed complicated signal patterns, and no evidence was obtained for the expected capped subporphyrin. Although two intense cation peaks at  $m/z$  911.3 and 929.1, which can be assigned to borenium cations of the doubly linked dyad  $[\mathbf{8}+\mathbf{1}-\text{OMe}-2\text{H}_2\text{O}]^+$  and the singly linked



Scheme 2. Synthetic routes to *meso*-tris(3-aminophenyl) substituted subporphyrin **8**. dba = dibenzylideneacetone.

dyad  $[\mathbf{8}+\mathbf{1}-\text{OMe}-\text{H}_2\text{O}]^+$  ( $\text{C}_{63}\text{H}_{44}\text{BN}_6\text{O}=911.37$  and  $\text{C}_{63}\text{H}_{46}\text{BN}_6\text{O}_2=929.38$ ), respectively, were observed in the MALDI-TOF mass spectrum of the reaction mixture, signals due to the triply linked Schiff-base cage could not be recorded. These results indicated that the arm length of **1** was too short to link three *meso*-aryl substituents of **8**. Next, the capping reaction of **8** and **2** was examined. Compound **2** (1 equiv) in a small amount of  $\text{CH}_2\text{Cl}_2$  was added to a solution of **8** in a mixed solvent of  $\text{CH}_2\text{Cl}_2/i\text{PrOH}$  (v/v=4:1) in the presence of TFA (5 equiv) and the solution was stirred at room temperature for 1 day. MALDI-TOF mass analysis of the reaction solution exhibited an intense cation signal at  $m/z$  941.5, which corresponded to  $[\mathbf{8}+\mathbf{2}-\text{OMe}-3\text{H}_2\text{O}]^+$  (i.e.,  $[\mathbf{12}\text{-Schiff-OR}]^+$ ;  $\text{C}_{63}\text{H}_{42}\text{BN}_6\text{O}_3=941.34$ ). Without purification, this Schiff base cage was reduced with  $\text{NaBH}_3\text{CN}$  to give capped subporphyrin **12** in 80% yield (Scheme 3). Under the similar reaction conditions, tripodal aldehydes **3**, **4**, **5**, and **6** also afforded corresponding capped subporphyrins **13**, **14**, **15**, and **16** in 59, 58, 85, and 70% yields, respectively (Scheme 4).

It is noteworthy that capping reactions at high concentrations of **8** and tripodal aldehydes ( $\geq 0.5$  mM) resulted in the for-



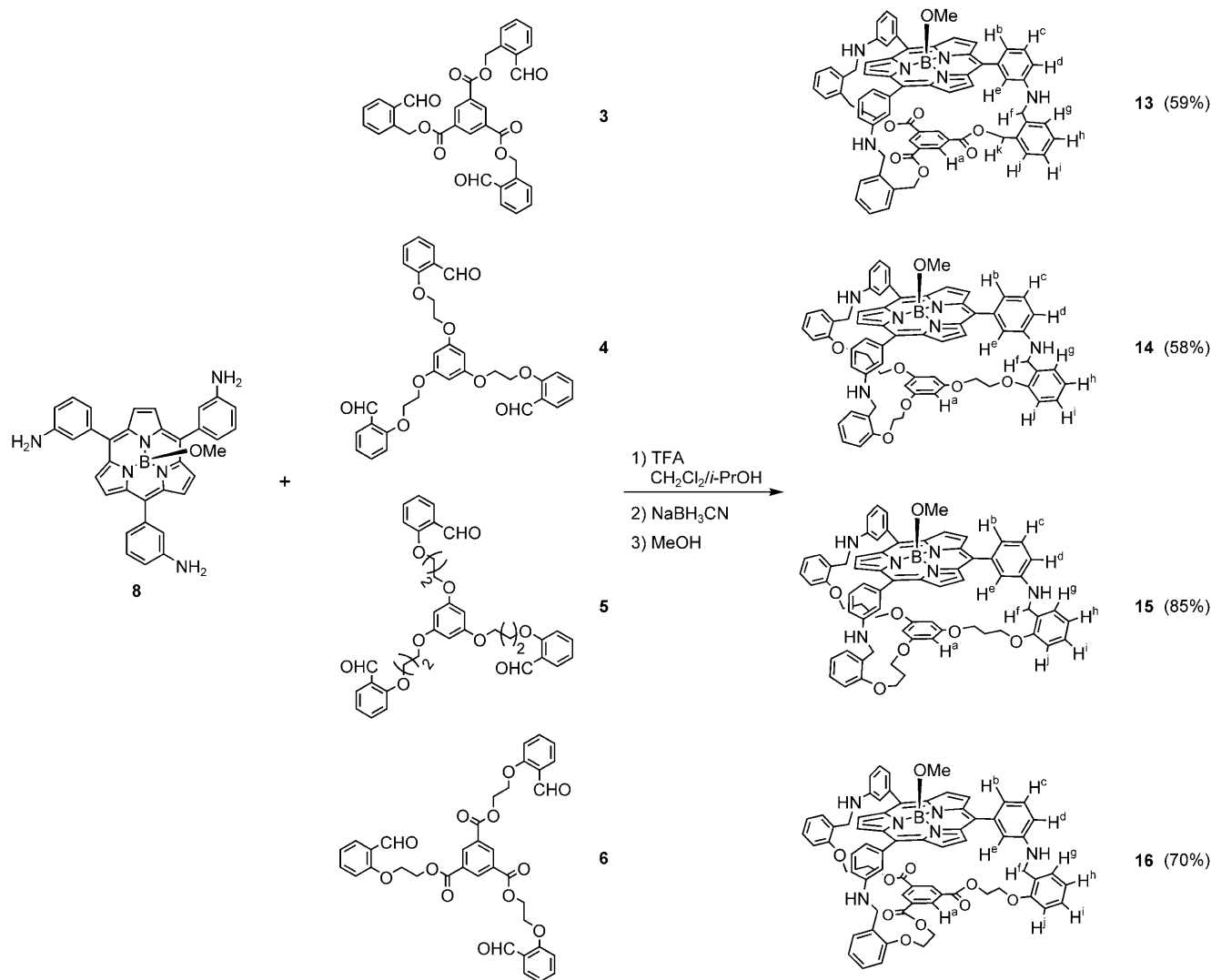
Scheme 3. Synthesis of capped subporphyrin **12**.

mation of orange precipitates of polymeric materials and the high yields of capped subporphyrins **12–16** were accomplished only in homogeneous solutions under dilute conditions (60  $\mu\text{M}$ ) without isolation of the Schiff bases. High-resolution electrospray ionization (HR-ESI) mass spectra of capped subporphyrins **12–16** exhibited intense boronium cation signals at  $m/z$  947.3884, 1031.3736, 1037.4205, 1079.4680, and 1121.4045, which correspond with the calculated values of  $[\text{M}-\text{OMe}]^+ = 947.3886$ , 1031.3733, 1037.4203, 1079.4673, and 1121.4051, respectively.

**X-ray crystallographic analysis:** The solid-state structures were unambiguously determined by X-ray diffraction analysis for capped subporphyrins **12**, **13**, **15**, and **16**. The bowl-shaped subporphyrin core of **12** was capped with the 1,3,5-triphenoxymethylbenzene moiety at the concave side. The average distance from the mean plane of the aryl ring of the cap to the  $\beta$  carbon atom of the subporphyrin is 3.56 Å.

Three *meso*-aryl rings of the subporphyrin tilt in the same direction, thus forming a helical structure. In the unit cell, two pairs of *P* and *M* spiral forms were found to construct a racemic crystal. Interestingly, the dihedral angles between the *meso*-aryl ring and the mean plane defined by six  $\beta$  carbon atoms are 52.1, 62.8, and 68.6°, which are distinctly larger than those of 2,6-unsubstituted aryl rings on subporphyrins, which are generally found to be in the range of 40–55°. This is explained in terms of the capping effect, which does not allow free rotation of the *meso*-aryl substituents, but rather forces them to adopt larger dihedral angles (Figure 1).

A single crystal of **13** suitable for X-ray analysis was grown from a mixture of DMSO/MeOH. The crystal structure of **13** also shows a spiral conformation similar to **12**. The tilting angles of the *meso*-aryl substituents are observed in the range of 43.1–54.6° with respect to the six  $\beta$  carbon mean plane. The average distance between the  $\beta$  carbon

Scheme 4. Synthesis of capped subporphyrins **13–16**.

mean plane and the aryl ring in the cap is only 3.15 Å, which is the shortest in the series, although the arm length of **13** (3 atoms) is longer than **12** (2 atoms). Such a remarkably short interplanar distance suggests considerable through-space  $\pi$ – $\pi$  interactions between the subporphyrin core and the cap. Although there are many examples of convex-to-plane- or concave-to-convex-type  $\pi$ – $\pi$  interactions in the solid state seen in fullerene–porphyrin cocrystals,<sup>[19]</sup> and belt- and bowl-shaped hydrocarbons,<sup>[20]</sup> such concave-to-plane-type  $\pi$ – $\pi$  interactions are rather rare.<sup>[21]</sup> This capped subporphyrin model might be a good platform to evaluate suitable interplanar separation or orientation of  $\pi$ –(concave)– $\pi$ (plane) interactions. Furthermore, in the helical structure of **13**, each of the three 1,2-phenylene rings in the bridging arms is located close to a  $\beta$ -C–H position. The distances from the mean plane of the 1,2-phenylene ring to the nearest  $\beta$  hydrogen atom are in the range of 2.59–2.75 Å and those to the nearest  $\beta$  carbon atom are in the range of 3.41–3.52 Å, indicating intramolecular CH– $\pi$  interactions.

Capped subporphyrin **15** was recrystallized from a mixture of  $\text{CHCl}_3/\text{MeOH}$  to afford single crystals of good quality (Figure 2A). The crystal structure of **15** also shows a concave-capped spiral structure. Two chloroform molecules used as the solvent were found close to **15** in the crystal lattice. Interestingly, one is placed at the center of the inner cavity of **15**, whereas the other is located between two *meso*-appended arm units. The chloroform molecule inside the cavity is orientationally disordered and the major orientation (62% occupancy) is shown in Figure 2A. In the other form, the chloroform molecule is arranged upside down with an occupancy of 38%. Owing to the long arm (5 atoms) and the chloroform clathration, the inner cavity of **15**· $\text{CHCl}_3$  is enlarged to be 6.7 Å in height.

A cubic crystal of **16** was obtained from a mixed solvent system of  $\text{CH}_2\text{Cl}_2/\text{mesitylene}/\text{MeOH}$  (Figure 2B). In the crystal structure, the axial methoxo ligand of **16** was hydrolyzed into the hydroxo form (i.e., **16-OH**) by adventitious water. Capped subporphyrin **16-OH** also exhibits a concave-

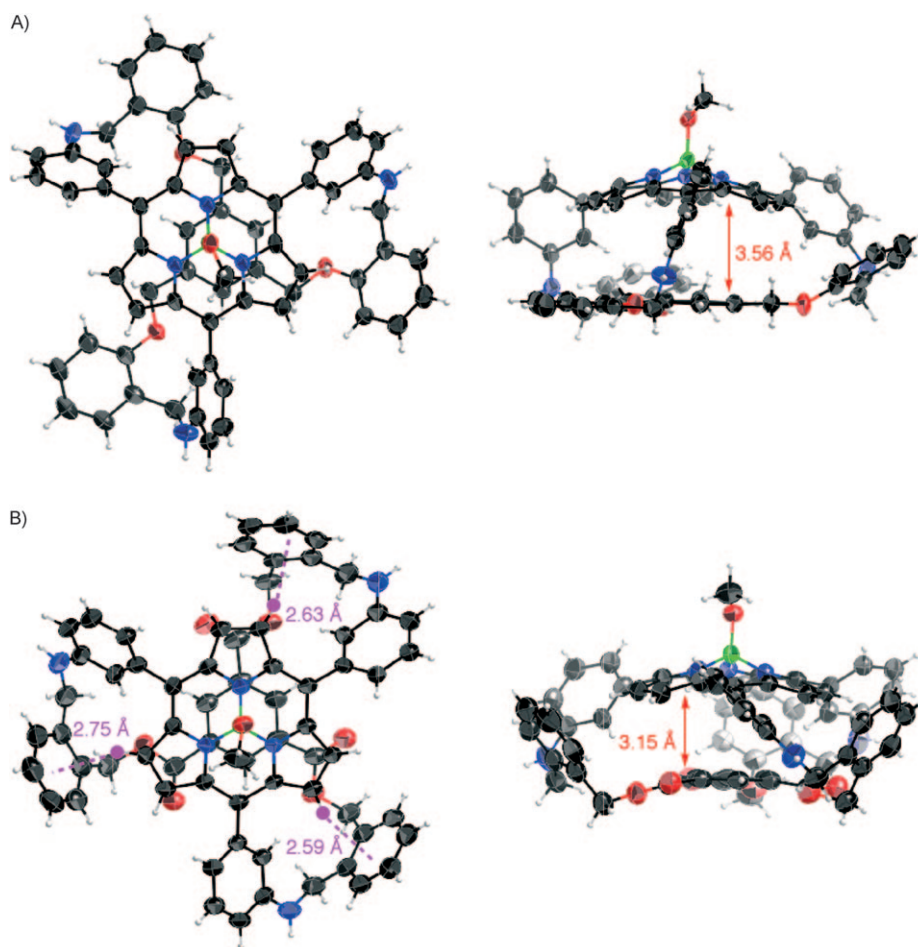


Figure 1. X-ray crystal structures of A) **12** and B) **13**.

capped, helical structure with pseudo- $C_3$  molecular symmetry<sup>[22]</sup> along the B–O bond axis. In this crystal structure, one mesitylene molecule is precisely packed in the cavity of **16-OH**, and three mean planes of the aryl ring of the cap, mesitylene, and six  $\beta$  carbon atoms of the subporphyrin are arranged in a parallel manner. The interplanar distances are 3.46 Å between the aryl ring of the cap and mesitylene and 3.16 Å between the six  $\beta$  carbon mean plane and mesitylene, suggesting favorable  $\pi$ – $\pi$  stacking between the three aromatic segments. Interestingly, the interplanar distance between the mesitylene and the subporphyrin core in **16-OH** is quite similar to that between the aryl ring of the cap and the subporphyrin core in **13**, which might suggest a suitable interplanar separation of around 3.15 Å for the favorable  $\pi$ – $\pi$  (concave)– $\pi$  (plane) stacking of capped subporphyrins. The inner cavity height of **16-OH** mesitylene is thus 6.6 Å, which is similar to that of **15**CHCl<sub>3</sub>. The dihedral angles of the *meso*-aryl rings of **15**CHCl<sub>3</sub> are in the range of 45.4–60.2° and those of **16-OH** mesitylene are 51.3° each with respect to the six  $\beta$  carbon mean plane, which are slightly smaller than those of **12**. To evaluate the affinity of mesitylene for the cavity of capped subporphyrin **16** in solution, a <sup>1</sup>H NMR titration experiment was carried out by the addi-

tion of excess amounts of mesitylene in CDCl<sub>3</sub> at room temperature. However, the proton signals due to **16** did not undergo any specific shift, even in the presence of a large excess amount of mesitylene. We also attempted <sup>1</sup>H NMR, UV/Vis absorption, and fluorescence titration analyses with **15** and **16** in the presence of  $C_3$  symmetric guests, for example, 1,3,5-trimethoxybenzene, 1,3,5-tribromobenzene, chloroform, and triphenylphosphane, but, none of them exhibited a particular affinity towards the cavities. These results suggested that the affinity and selectivity of these guest molecules toward the inner cavities of **15** and **16** in solution were poor. Nevertheless, the solid-state structures of **15**CHCl<sub>3</sub> and **16-OH** mesitylene indeed demonstrated the encapsulating ability of capped subporphyrins, encouraging their use as a host for a guest with  $C_3$ -molecular symmetry. In addition, we have recently disclosed characteristic structural changes for the *meso*-[4-(*N,N*-dibenzylaminophenyl)]-substituted subporphyrins, in which

slight but distinctive benzoquinone-type bond length alternations have been observed for *meso*-attached benzene rings.<sup>[6]</sup> However, such remarkable bond length discriminations are not confirmed for capped subporphyrins **12**, **13**, **15**CHCl<sub>3</sub>, and **16-OH** mesitylene, which suggests little influence of 3-aminophenyl groups on the electronic properties of the subporphyrin core in the ground state.

**<sup>1</sup>H NMR spectroscopy:** The <sup>1</sup>H NMR spectrum of **12** shows a  $C_3$ -symmetric signal pattern featuring two singlets at  $\delta$  = 5.77 and 7.52 ppm due to the aryl protons of the cap ( $H^a$ , designated in Scheme 3) and the  $\beta$ -pyrrolic protons at room temperature, both of which are significantly high-field shifted compared with those of the fragment molecules **2** and **8**. On the basis of the crystal structure, the former high-field shift can be ascribed to the diatropic ring-current effect of the 14 $\pi$ -aromatic subporphyrin core and the latter is understandable in terms of the local ring current of the 1,2-phenylene moiety of the bridging arm. Similar spectral patterns were observed for **14**, **15**, and **16** in CDCl<sub>3</sub>, in which the pyrrolic  $\beta$  protons were observed at  $\delta$  = 7.78, 7.28, and 7.27 ppm, respectively, as a sharp singlet. The aryl protons ( $H^a$ ) of the cap are observed at  $\delta$  = 5.54, 5.51, and 8.40 ppm

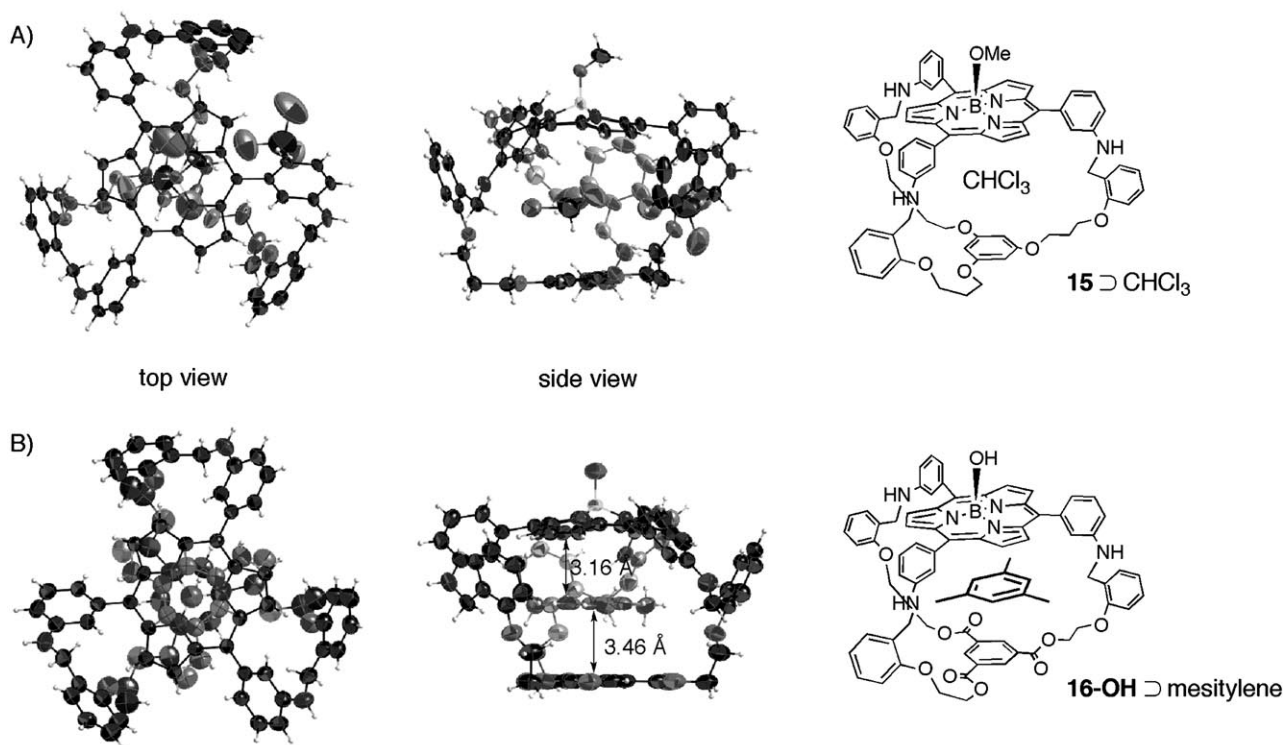


Figure 2. X-ray crystal structures of capped subporphyrin A) **15**  $\supset$   $\text{CHCl}_3$  and B) **16-OH**  $\supset$  mesitylene. Only the major orientation of disordered chloroform molecule inside the cavity is shown for (A).

for **14**, **15**, and **16**, respectively, with high-field shifts compared with those of **4**, **5**, and **6** observed at  $\delta=6.19$ , 6.09, and 8.87 ppm. These data indicated the influences of the diatropic ring currents, similar to the case of **12**. Such shielding effects for the cap proton  $\text{H}^a$  decreased in the order of **12**  $\gg$  **14**  $>$  **15**  $>$  **16** ( $\Delta\delta=1.75$ , 0.65, 0.58, and 0.47 ppm, respectively), probably reflecting the average distance between the cap and the subporphyrin core. With the solid-state structures and the observed single sets of  $^1\text{H}$  NMR spectroscopy signals, the capping reaction has been concluded to occur with complete concave-face selectivity for **12**, **15**, and **16**. The similar  $^1\text{H}$  NMR spectroscopy data of **14** strongly suggested the same concave-capped structure. The concave-capping selectivity can be readily ascribed to considerable steric effects exerted by the axially coordinated boron ligand at the convex face. Generally the solubilities of capped subporphyrins are much lower than **8**. Particularly, the solubility of **13** is very poor, which does not allow us to detect a clear  $^1\text{H}$  NMR spectrum in  $\text{CDCl}_3$ .

**Spiral interconversion: VT-NMR spectroscopy:** In the meantime, we found that **13** was reasonably soluble in DMSO and then examined a  $^1\text{H}$  NMR spectrum in  $[\text{D}_6]\text{DMSO}$ . At room temperature, the  $^1\text{H}$  NMR spectrum of **13** exhibited a  $C_3$ -symmetric signal pattern, featuring a singlet due to the aryl cap  $\text{H}^a$  proton at  $\delta=6.56$  ppm, which undergoes the largest high-field shift in the series ( $\Delta\delta=2.14$  ppm) compared with trialdehyde **3**. Interestingly, signals due to the  $\beta$  and benzyl protons  $\text{H}^f$  and  $\text{H}^k$  (see Scheme 4) resonate as

pairs of split two peaks at  $\delta=7.17$  and 6.00, 4.73 and 4.70, respectively. In particular, the signals due to  $\text{H}^k$  displayed a clear geminal coupling feature with  $J_{\text{gem}}=10.1$  Hz (Figure 3A). The large difference in chemical shifts of the two  $\beta$ -proton signals indicated their magnetically nonequivalent environments, hence supporting a  $C_3$ -symmetrical helical structure of **13** in solution, similar to that found in the crystal structure. The high-field shifted signal at  $\delta=6.00$  ppm has been assigned to the  $\beta$  protons close to the 1,2-phenylene rings in the bridge (magenta in the top view of Figure 1B). Similarly, separated signals due to  $\text{H}^f$  and  $\text{H}^k$  can be explained in terms of a spiral conformation of **13**. The NOESY spectrum of **13** in  $[\text{D}_6]\text{DMSO}$  at room temperature also indicates a helical structure, featuring through-space proton correlations between the cap  $\text{H}^a$  and *meso*-aryl  $\text{H}^e$  protons, and the  $\beta$  proton at  $\delta=6.00$  ppm and  $\text{H}^h$  or  $\text{H}^i$ . In particular, the strong correlation between  $\text{H}^a$  and  $\text{H}^e$  is indicative of close stacking between the aryl ring of the cap and the subporphyrin core in solution. These  $^1\text{H}$  NMR spectral features of **13** are different from those of **12**, **14**, **15**, and **16**, since the  $\beta$ - and benzylic protons in **12**, **14**, **15**, and **16** are recorded as sharp and coalesced signals in  $\text{CDCl}_3$  at room temperature (see Figure S1 in the Supporting Information), despite their spiral crystal structures. Since subporphyrins **12**, **14**, **15**, and **16** exhibit essentially the same  $^1\text{H}$  NMR spectral pattern in  $[\text{D}_6]\text{DMSO}$ , showing sharp  $\beta$ -proton signals at  $\delta=7.32$ , 7.47, 7.29, and 7.17 ppm, respectively, and coalesced benzylic protons due to  $\text{H}^f$  and  $\text{H}^k$ , the solvent effect would be marginal. It can be considered that

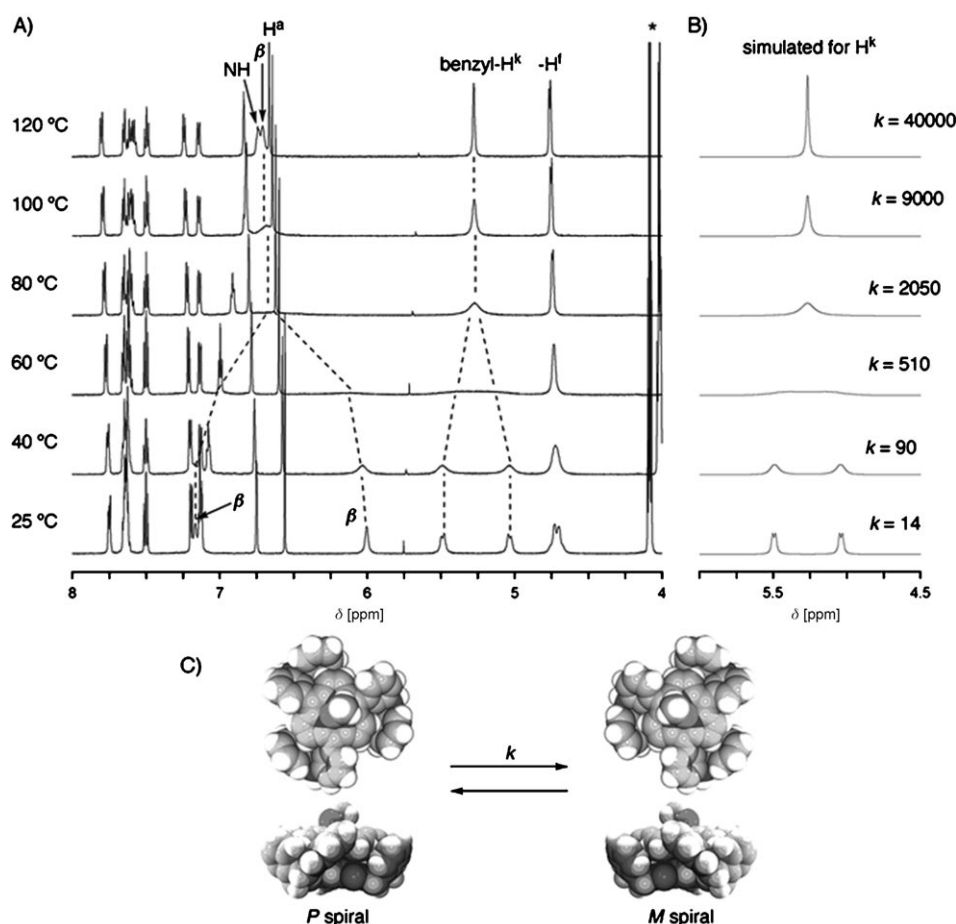


Figure 3. a) 600 MHz VT- $^1\text{H}$  NMR spectra of **13** in  $[\text{D}_6]\text{DMSO}$  (\*: solvent peaks), b) simulated  $^1\text{H}$  NMR spectra for  $\text{H}^k$ , and c) interconversion between the *P* and *M* spiral forms.

rotational freedom of the *meso*-aryl groups is considerably suppressed in **12–16** due to the cap that connects to three *meso*-aryl substituents. Thus, the unique  $^1\text{H}$  NMR spectral features of **13** may be assigned to a small exchange rate of two spiral conformations, that is, *P* and *M* spiral (Figure 3C) with respect to the  $^1\text{H}$  NMR timescale, whereas such exchange rates are likely to be larger than the  $^1\text{H}$  NMR timescale for the other capped subporphyrins **12**, **14**, **15**, and **16**.

To verify this hypothesis, variable-temperature (VT)  $^1\text{H}$  NMR spectra of **12**, **13**, and **16** were examined. Upon increasing the temperature, the split signals due to the  $\beta$ -,  $\text{H}^f$ , and  $\text{H}^k$  protons of **13** indeed showed significant peak broadening and finally coalesced at  $120^\circ\text{C}$  into sharp singlets at  $\delta = 6.71$  and  $5.28$  ppm due to the  $\beta$ - and  $\text{H}^f$  protons, and a doublet ( $J(\text{CH}_2, \text{NH}) = 5.5$  Hz) at  $4.75$  ppm due to  $\text{H}^k$  (Figure 3). The other proton signals, such as  $\text{H}^a$ – $\text{H}^c$ , and  $\text{H}^g$ – $\text{H}^j$ , did not exhibit any characteristic shift or coalescence behavior and the total molecular symmetry of  $C_3$  was preserved in a range from  $25$  to  $140^\circ\text{C}$ . The temperature-dependent spectral changes of the  $\beta$ -,  $\text{H}^f$ , and  $\text{H}^k$  protons are reversible and the original spectrum of **13** was completely recovered upon cooling to room temperature. During the measurement, a sharp singlet due to the axial methoxo pro-

tons was observed at  $\delta = -0.03$  to  $0.08$  ppm in the same signal intensity almost independently of the temperature. Thus, the observed dynamic motion of **13** is neither bowl-to-bowl inversion nor an axial-ligand exchange reaction, but interconversion of the helical structures with temperature-dependent exchange rates. The exchange rates of **13** were estimated to be  $k = 14, 90, 510, 2050, 9000,$  and  $40000$   $\text{s}^{-1}$  at  $25, 40, 60, 80, 100,$  and  $120^\circ\text{C}$ , respectively, by simulating the NMR spectroscopy signal patterns for the benzyl proton  $\text{H}^k$ .

In the cases of **12** and **16**, similar spectral changes were observed in  $\text{CD}_2\text{Cl}_2$  upon decreasing the temperature (Figure 4 and the Supporting Information). The capped subporphyrin **12** exhibited sharp signals due to the  $\beta$ -, benzyl- $\text{H}^f$  and  $\text{H}^k$  protons at  $\delta = 7.48, 4.41,$  and  $3.89$  ppm, respectively, at  $25^\circ\text{C}$  in  $\text{CD}_2\text{Cl}_2$ . These peaks were separated into three pairs of two broad signals at  $-75^\circ\text{C}$  as shown in Figure 4A. The six  $\beta$  protons of **12** resonated at  $\delta = 7.73$  and  $7.12$  ppm at

$-90^\circ\text{C}$ , each signal corresponded to three protons. The  $^1\text{H}$  NMR spectroscopy simulations were performed for  $\text{H}^f$  and  $\text{H}^k$  in the range from  $-90$  to  $-15^\circ\text{C}$ , which allowed the estimation of the temperature-dependent exchange rate constants as  $k = 100$  to  $35000$   $\text{s}^{-1}$  (Figure 4B). Signals due to the  $\beta$ -,  $\text{H}^f$ , and ethylene chain protons of **16** also exhibited significant broadening at  $-70^\circ\text{C}$  in  $\text{CD}_2\text{Cl}_2$ . Finally at  $-90^\circ\text{C}$ , the signals of the  $\beta$  protons were divided into two parts at  $\delta = 7.25$  and  $6.81$  ppm, which were well reproduced by the simulated spectra with  $k = 80$   $\text{s}^{-1}$  (Figure S3 in the Supporting Information).

The exchange rate constants of **12**, **13**, and **16** were analyzed by Eyring plots, in which these capped subporphyrins displayed good linear correlations (Figure 5). The activation parameters of **13** in DMSO were calculated to be  $\Delta H^\ddagger = 76.4$   $\text{kJ mol}^{-1}$  and  $\Delta S^\ddagger = 34.5$   $\text{J mol}^{-1} \text{K}^{-1}$ , hence, the energy barrier of the interconversion between the *P* and *M* spiral forms was estimated to be  $\Delta G^\ddagger_{298} = 66.1$   $\text{kJ mol}^{-1}$  at  $25^\circ\text{C}$ .

Table 1 summarizes the activation parameters thus calculated for **12**, **13**, and **16**. Interestingly, a negative value of  $-45.7$   $\text{J mol}^{-1} \text{K}^{-1}$  was obtained for the entropy change of **12**, while the other two subporphyrins exhibited positive  $\Delta S^\ddagger$  values. This can be simply explained in terms of the short

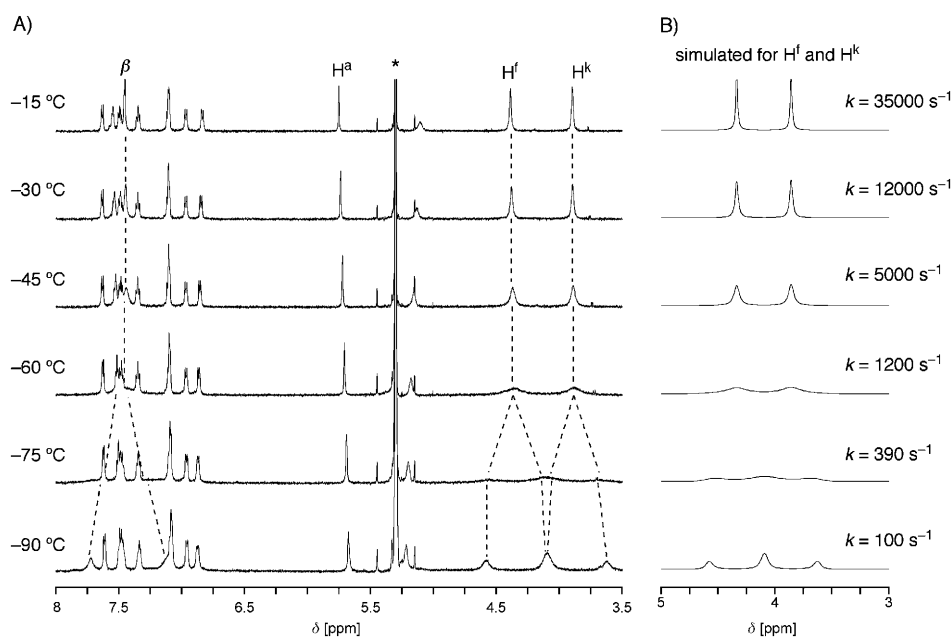


Figure 4. a) 600 MHz VT- $^1\text{H}$  NMR spectra of **12** in  $\text{CD}_2\text{Cl}_2$  (\*: solvent peaks), and b) simulated  $^1\text{H}$  NMR spectra for benzylic proton  $\text{H}^f$  and  $\text{H}^k$ .

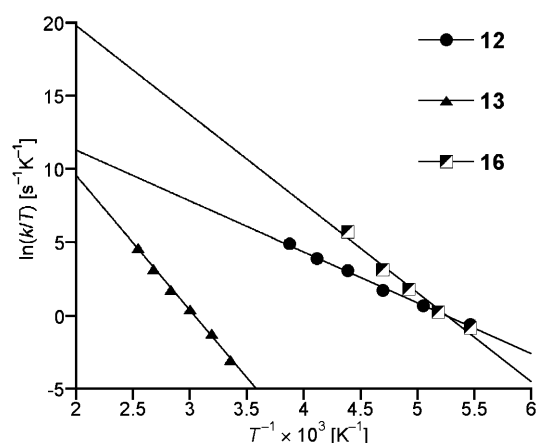


Figure 5. Eyring plots for capped subporphyrins **12**, **13**, and **16**.

arm length. In the transition state, it is expected that the *meso*-aryl substituents are arranged in an almost perpendicular manner with respect to the subporphyrin mean plane, and the distance from the aryl ring of the cap to the subporphyrin core is longer than that of the spiral forms. In case of **12**, such conformational change results in the formation of a tight transition structure in which the free motion of the linker unit is restricted and three *meso*-aryl rings are forced to synchronize the tilting behavior due to the short strap. In contrast, capped subporphyrins **13** and **16**, bearing longer arms, are expected to obtain the degree of freedom in the transition structures rather than their spiral forms. Such influences of the arm length on the structure can be seen in their dihedral angles of *meso*-aryl rings in the solid state. Significantly large dihedral angles of **12** in the crystal struc-

ture also indicate its structural tightness. The largest  $\Delta H^\ddagger$  and the energy barrier  $\Delta G^\ddagger_{298}$  were obtained for **13**. Considering the crystal structure, through-space interactions between the aryl ring of the cap and the subporphyrin core along with characteristic intramolecular  $\text{CH}-\pi$  interactions presumably play an important role in stabilizing the spiral conformation. It is worth noting that the  $\Delta H^\ddagger$  value of subporphyrin **16** ( $50.4 \text{ kJ mol}^{-1}$ ) is considerably larger than that of **12** ( $28.9 \text{ kJ mol}^{-1}$ ). Although the resulting  $\Delta G^\ddagger_{298}$  of **16** is the smallest in the series due to its positive large entropy factor; this result might suggest favorable interactions between the 1,3,5-tri(alkoxycarbonyl)benzene moiety and subporphyrin

Table 1. Structural data and activation parameters<sup>[a]</sup> of spiral motion of **12**, **13**, and **16**.

	<b>12</b>	<b>13</b>	<b>16</b>
arm length <sup>[b]</sup>	2 atoms	3 atoms	5 atoms
aryl cap			
tilting angles <sup>[c]</sup> [°]	52.1	43.1	51.3
	62.8	46.0	51.3
	68.6	54.6	51.3
$\Delta H^\ddagger$ [ $\text{kJ mol}^{-1}$ ]	28.9	76.4	50.4
$\Delta S^\ddagger$ [ $\text{J mol}^{-1} \text{K}^{-1}$ ]	-45.7	34.5	67.9
$\Delta G^\ddagger_{298}$ [ $\text{kJ mol}^{-1}$ ]	43.5	66.1	30.2
$k_{298}$ [ $\text{s}^{-1}$ ] <sup>[d]</sup>	$2.2 \times 10^5$	16	$3.2 \times 10^7$

[a] Activation parameters were calculated by simulating the VT- $^1\text{H}$  NMR spectra of **12** and **16** in  $\text{CD}_2\text{Cl}_2$  and **13** in  $[\text{D}_6]\text{DMSO}$ . [b] Number of linker atoms between the aryl group of the cap and the 1,2-phenylene ring. [c] Dihedral angles between the *meso*-aryl ring and the mean plane of six  $\beta$  carbon atoms in the crystal structure. The tilting angle of **16** was calculated from the structure of **16-OH** mesitylene. [d] Exchanging rate constant between *P* and *M* spiral forms at 298 K. These values were calculated based on the Eyring equation.

core rather than 1,3,5-trialkoxymethylbenzene analogue in the capped system. In short, the dynamic spiral interconversion can be controlled entropically by arm length and enthalpically by intramolecular interactions between the subporphyrin core and the aryl ring of the cap. Such an adjustable feature of dynamic spiral interconversion is quite important both for biological movements<sup>[23]</sup> and for constructing

artificial nanomachines.<sup>[24]</sup> In this view, capped subporphyrins are also a promising platform owing to their highly tunable properties.

**Optical properties:** The UV/Vis absorption spectra of subporphyrins **8** and **12–16** recorded in CH<sub>2</sub>Cl<sub>2</sub> are shown in Figure 6A. Recently, we have reported largely perturbed op-

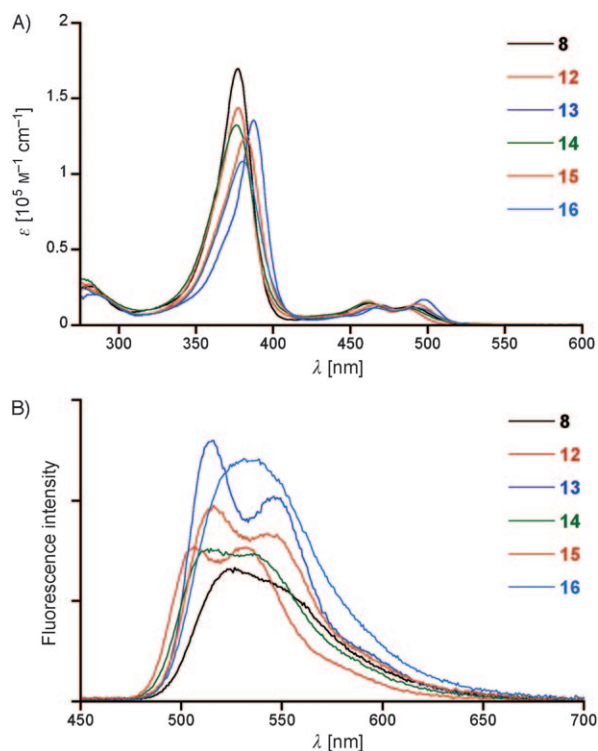
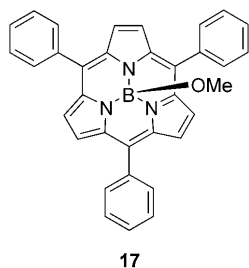


Figure 6. A) UV/Vis absorption spectra and B) fluorescence spectra of **8** and **12–16** in CH<sub>2</sub>Cl<sub>2</sub>. Fluorescence spectra were recorded by excitation at the absorption maxima (377–382 nm).

tical properties of *meso*-(4-(*N,N*-dialkylamino)phenyl)-substituted subporphyrins<sup>[6]</sup> which exhibited redshifted absorption spectra and intensified fluorescence compared with *meso*-triphenyl-substituted subporphyrin (**17**). Contrary to these 4-aminophenyl-substituted analogues, 3-aminophenyl-substituted subporphyrin **8** shows only modest changes in the absorption and fluorescence spectra. This difference can be attributed to small conjugative interaction of 3-aminophenyl substituent. Since the capping reaction can be considered merely as an *N*-alkylation reaction at the *meso*-substituted 3-aminophenyl groups, the direct  $\pi$ -electronic impact of the cap to the subporphyrin core should be trivial. In fact, the spectral shapes of capped subporphyrins **12** and **14** are analogous to that of **8**, although slight broadening of the Soret-like band was observed. In the ab-



sorption spectra of the capped subporphyrins **15** and **16**, with five atom arms, much broader and redshifted Soret-like bands were observed at 382 and 380 nm, respectively. The fluorescence spectra of **12** and **15** displayed rather distinguishable vibronic structures at 507 and 532 nm, and 517 and 544 nm, respectively, whereas **14** and **16** have ill-defined spectral shapes as well as non-capped subporphyrin **8**. These minor differences in the absorption and fluorescence spectra can be attributed to the conformational properties, such as structural rigidity, restriction of the free rotation of *meso*-aryl rings, and solvent accessibility into the cavity. The most significant perturbation was found in the absorption spectrum of **13**, in which a sharp Soret-like band was recorded at 387 nm with the largest bathochromic shift in the series. Besides, the Q(0,0) band of **13** also exhibits a characteristic redshift to 497 nm with concurrent enhancement. Interestingly, the fluorescence spectrum of **13** shows a fine vibronic structure with band peaks at 515 and 546 nm. The Stokes shift of **13** thus calculated is 703 cm<sup>-1</sup>, which is the smallest in the series, indicating its rigid structure in the excited state. The fluorescence quantum yields of capped subporphyrins are comparable to that of the mother subporphyrin **8** (Table 2). However, those of 1,3,5-tri(alkoxycarbonyl)benzene-capped subporphyrins **13** and **16** are slightly but distinctively enhanced compared with **8**.

Table 2. Optical properties of subporphyrins **8** and **12–16**.

	Absorption		Fluorescence		Stokes shift [cm <sup>-1</sup> ]
	Soret [nm]	Q(0,0) [nm]	$\lambda_{\max}$ [nm]	$\Phi_F$ [%]	
<b>8</b>	377	489	525	12.2	1402
<b>12</b>	377	487	507	13.2	810
<b>13</b>	387	497	515	16.6	703
<b>14</b>	377	487	515	13.3	1116
<b>15</b>	382	493	517	15.6	942
<b>16</b>	380	492	534	16.7	1598

**DFT calculations:** DFT calculations were performed for **8**, **12**, and **13** at the B3LYP/6-31G(d) level by using the Gaussian 03 package (Figure 7).<sup>[25]</sup> The optimized structures of **12** and **13** were calculated based on their crystal structures (data shown in Table 3 and the structure of **8** was generated from the crystal structure of *meso*-triphenylsubporphyrin **17**). Subporphyrin **8** has four frontier orbitals similar to **17**. Capped subporphyrin **12** also provides a similar four orbital set, which is indicative of a small direct influence of the cap on the electronic properties of the subporphyrin core in the ground state. Unlike **8** and **12**, four vacant orbitals were found for capped subporphyrin **13** in a similar energy range, along with a couple of degenerated HOMOs. The orbital coefficients in the LUMO and LUMO+1 of **13** are localized at the aryl ring of the cap (Figure 7). LUMO+2 and LUMO+3 correspond to the uncapped e orbitals due to the subporphyrin core. Namely, LUMO levels of the electron-deficient 1,3,5-tri(alkoxycarbonyl)benzene moiety are slightly lower than those of *meso*-(3-aminophenyl)subporphyrin. For comparison, frontier orbital energy levels of the

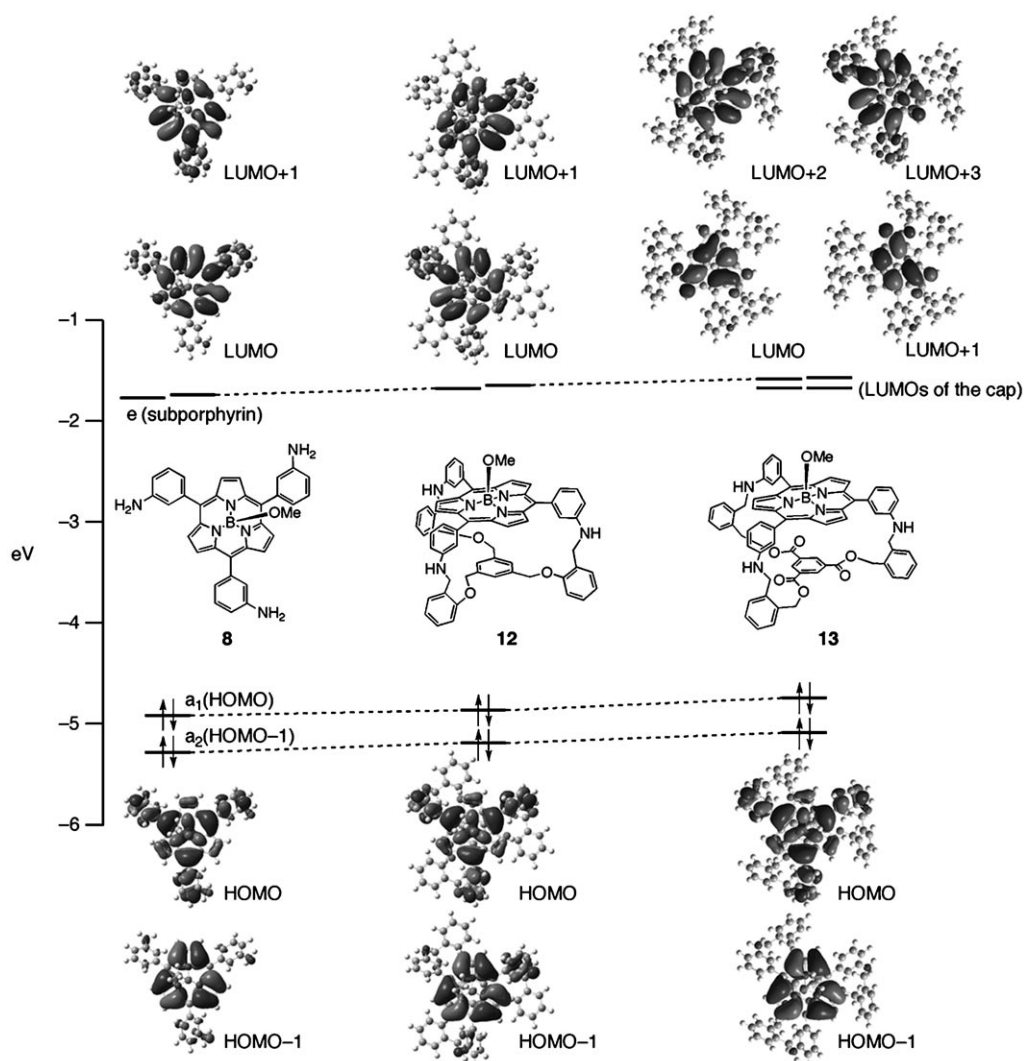


Figure 7. Molecular orbital (MO) diagrams of **8**, **12**, and **13**. MOs of LUMO and LUMO+1 for **13** are localized on the aryl rings of the cap, therefore, the orbital diagrams are drawn as bottom views.

cap units of **12–16**, that is, 1,3,5-triphenoxymethylbenzene (**18**), 1,3,5-trimethoxybenzene (**19**), and trimethylbenzene-1,3,5-tricarboxylate (**20**), were calculated at the B3LYP/6-31G(d) level (Figure S4 in the Supporting Information). The energy levels of the HOMOs for **18–20** are considerably lower than that of subporphyrin **8**. Also, the LUMO of **20** is coincidentally similar in energy to that of **8** because of three electron-withdrawing ester groups. Although any significant orbital overlap or hybridization between the cap unit and the subporphyrin core were not found in the calculated MOs,<sup>[26]</sup> such low-lying LUMOs of the cap would be advantageous for through-space  $\pi$ - $\pi$  interactions with the concave surface of the subporphyrin core, as observed in the absorption spectrum of **13**. In a previous report, similar absorption spectral changes have been observed for a capped porphyrin with an electron-deficient cap.<sup>[27]</sup> Judging from the experimental and theoretical results, weak incipient charge-transfer interactions can also be expected for capped subporphyrin **13**. In addition, similar cap-dependent unoccupied orbitals

were found in the LUMO and LUMO+1 of subporphyrin **16**. The observed absorption spectrum of **16**, however, did not exhibit characteristic spectral changes compared with **13**. It is more likely that the spectral shape of **16** is rather similar to that of **15** despite the difference in the aryl ring of the cap. This situation suggests that structural restraints and dynamic motions in solution based on the arm length are particularly important to induce efficient through-space interactions between the cap and the core as well as its  $\pi$ -electronic characters.

## Conclusions

Capped subporphyrins **12–16** were synthesized in good yields from **8** and tripodal trialdehydes **2–6**. The complete concave-face selectivity of these capping reactions was unambiguously confirmed by <sup>1</sup>H NMR spectroscopy and X-ray crystallographic analysis. Capped subporphyrins **15** and **16**,

Table 3. Crystallographic data for compounds **12**, **13**, **15**⊃CHCl<sub>3</sub>, and **16-OH**⊃mesitylene.

	<b>12</b>	<b>13</b>	<b>15</b> ⊃CHCl <sub>3</sub>	<b>16-OH</b> ⊃mesitylene
formula	C <sub>66</sub> H <sub>51</sub> B <sub>1</sub> N <sub>6</sub> O <sub>4</sub> · 2CH <sub>2</sub> Cl <sub>2</sub>	C <sub>67</sub> H <sub>51</sub> B <sub>1</sub> N <sub>6</sub> O <sub>7</sub> · C <sub>2</sub> H <sub>6</sub> S <sub>1</sub> O <sub>1</sub> ·C <sub>1</sub> H <sub>4</sub> O <sub>1</sub>	C <sub>70</sub> H <sub>63</sub> B <sub>1</sub> N <sub>6</sub> O <sub>7</sub> ·CHCl <sub>3</sub> , 0.8CHCl <sub>3</sub> , CH <sub>3</sub> OH	C <sub>69</sub> H <sub>55</sub> B <sub>1</sub> N <sub>6</sub> O <sub>10</sub> ·C <sub>9</sub> H <sub>12</sub>
crystal size [mm]	0.20 × 0.20 × 0.10	0.40 × 0.30 × 0.20	0.65 × 0.30 × 0.20	0.35 × 0.35 × 0.20
formula weight	1148.77	1173.12	1356.44	1259.19
crystal system	monoclinic	monoclinic	orthorhombic	cubic
space group	<i>P2<sub>1</sub>/n</i>	<i>C2/c</i>	<i>Pbca</i>	<i>Pa-3</i>
<i>a</i> [pm]	16.799(5)	30.0417(11)	16.7601(15)	23.300(3)
<i>b</i> [pm]	22.051(7)	17.2535(19)	20.6452(18)	23.300(3)
<i>c</i> [pm]	17.270(5)	29.0055(18)	38.996(3)	23.300(3)
<i>α</i> [°]	90	90	90	90
<i>β</i> [°]	118.974(10)	108.808(3)	90	90
<i>γ</i> [°]	90	90	90	90
<i>V</i> [nm <sup>3</sup> ]	5597(3)	14231.5(19)	13493(2)	12649(3)
<i>Z</i>	4	8	8	8
<i>T</i> [K]	123(2)	123(2)	90(2)	123(2)
$\rho_{\text{calcd}}$ [mgm <sup>-3</sup> ]	1.363	1.095	1.335	1.322
total reflns	9689	16052	11880	3707
unique reflns	5895	8003	7957	1654
$\mu$ [mm <sup>-1</sup> ]	0.269		0.101	0.088
<i>R</i> <sub>1</sub> [ <i>I</i> > 2 $\sigma$ ( <i>I</i> )]	0.0753	0.0859	0.0981	0.0995
<i>wR</i> <sub>2</sub> (all data)	0.1278	0.1564	0.3063	0.1920
GOF	1.022	0.958	1.035	1.041
CCDC <sup>[a]</sup> number	720912	720913	720914	720915

[a] CCDC-720912, 720913, 720914, and 720915 contain the supplementary crystallographic data for this paper. These data can be obtained free of charge from The Cambridge Crystallographic Data Centre via [www.ccdc.cam.ac.uk/data\\_request/cif](http://www.ccdc.cam.ac.uk/data_request/cif).

with an arm length of five atoms, have large inner cavities that are enough to encapsulate solvent molecules, such as mesitylene and chloroform. On the other hand, capped subporphyrins **12** and **13** exhibit rather tight structures, in which the cap units are closely stacked to the subporphyrin core. In particular, the intramolecular  $\pi$ - $\pi$  interactions and multiple CH- $\pi$  interactions of **13** result in a drastic decrease in the exchange rate between the *P* and *M* spiral forms in solution compared with **12** and **16**. Besides, the through-space intramolecular interactions of **13** lead to the remarkable perturbations in the absorption spectrum. MO calculations also suggested favorable orbital interactions between the subporphyrin core and the cap through the low-lying LUMOs of the 1,3,5-tri(alkoxycarbonyl)benzene moiety. Further fabrication of capped subporphyrins are actively in progress in our laboratory.

## Experimental Section

**General:** All reagents and solvents were of commercial reagent grade and were used without further purification. <sup>1</sup>H, <sup>11</sup>B, and <sup>13</sup>C NMR spectra were recorded on a JEOL delta-600 spectrometer, and chemical shifts were reported on the delta scale in ppm relative to internal standards CHCl<sub>3</sub> ( $\delta$  = 7.26 ppm for <sup>1</sup>H, 77.16 ppm for <sup>13</sup>C), CH<sub>2</sub>Cl<sub>2</sub> ( $\delta$  = 5.30 ppm for <sup>1</sup>H), DMSO ( $\delta$  = 2.50 ppm for <sup>1</sup>H), and an external standard BF<sub>3</sub>·OEt<sub>2</sub> in CDCl<sub>3</sub> ( $\delta$  = 0.00 ppm for <sup>11</sup>B)). Spectroscopic grade solvents were used for all spectroscopic studies without further purification. UV/Vis absorption spectra were recorded on a Shimadzu UV-3100 spectrometer. Fluorescence spectra were recorded on a Hamamatsu Photonics C9920-02 spectrometer and absolute fluorescence quantum yields were measured by a photon-counting method using an integration sphere. ESI-TOF mass spectra were recorded on a Bruker Daltonics micro TOF LC instrument

using positive-ion mode. Preparative separations were performed by silica gel gravity column chromatography (Wako gel C-300) or size-exclusion gel permeation chromatography (GPC) (Bio-Rad Bio-Beads S-X1, packed with THF in a 8 × 50 or 4 × 90 cm gravity column). Crystallographic data were collected on a Rigaku R-AXIS RAPID diffractometer with graphite monochromated MoK $\alpha$  radiation ( $\lambda$  = 0.71075 Å) at -150 °C (for **12**, **13**, and **16-OH**⊃mesitylene) or on a Bruker SMART APEX with graphite monochromated MoK $\alpha$  radiation ( $\lambda$  = 0.71073 Å) at -183 °C (for **15**⊃CHCl<sub>3</sub>).

**Methoxo(5,10,15-tri(3-nitrophenyl)subporphyrinato)boron(III) (9):** This compound was synthesized from pyridine tri-*N*-pyrrolylborane (2.00 g, 6.94 mmol) and 3-nitrobenzaldehyde (3.10 g, 20.8 mmol) in the presence of TFA (0.75 mL) according to the general procedure for the synthesis of *meso*-triarylsbporphyrin. The product was purified by silica gel column chromatography (eluent: CH<sub>2</sub>Cl<sub>2</sub>/AcOEt = 95:5). Subsequent recrystallization from CH<sub>2</sub>Cl<sub>2</sub>/MeOH gave **9** as an orange powder (41 mg, 0.9%). <sup>1</sup>H NMR (600 MHz, CDCl<sub>3</sub>):  $\delta$  = 8.85 (s, 3H; *meso*-Ar-*o*-H), 8.50 (d, *J* = 7.4 Hz, 3H; *meso*-Ar-*o* or *p*-H), 8.43 (d, *J* = 7.4 Hz, 3H; *meso*-Ar-*o* or *p*-H), 8.14 (s, 6H;  $\beta$ -H), 7.92 (t, *J* = 7.4 Hz, 3H; *meso*-Ar-*m*-H), 0.82 ppm (s, 3H; axial-OMe); <sup>11</sup>B NMR (193 MHz, CDCl<sub>3</sub>):  $\delta$  = -15.4 ppm (s, 1B); <sup>13</sup>C NMR (150 MHz, CDCl<sub>3</sub>):  $\delta$  = 148.6, 141.4, 138.8, 138.5, 129.9, 127.4, 123.1, 122.7, 118.6, 46.8 ppm (axial-OMe); UV/Vis (in CH<sub>2</sub>Cl<sub>2</sub>):  $\lambda$  ( $\epsilon$ ) = 373 (141 000), 460 nm (14 000 M<sup>-1</sup> cm<sup>-1</sup>); fluorescence (in CH<sub>2</sub>Cl<sub>2</sub>,  $\lambda_{\text{ex}}$  = 373 nm):  $\lambda_{\text{max}}$  = 512 nm,  $\Phi_{\text{F}}$  = 8 × 10<sup>-3</sup>; HR-ESIMS-TOF (positive mode): *m/z* calcd for C<sub>33</sub>H<sub>18</sub>N<sub>6</sub>B<sub>1</sub>O<sub>6</sub>: 605.1381 [M-OMe]<sup>+</sup>; found: 605.1396.

**Methoxo(5,10,15-tri(3-bromophenyl)subporphyrinato)boron(III) (10):** This compound was synthesized from pyridine tri-*N*-pyrrolylborane (2.00 g, 6.94 mmol) and 3-bromobenzaldehyde (2.45 mL, 21.0 mmol) in the presence of TFA (1.03 mL) according to the general procedure. The product was purified by silica gel column chromatography (eluent: CH<sub>2</sub>Cl<sub>2</sub>/hexane/ether = 1:2:1). Subsequent recrystallization from CH<sub>2</sub>Cl<sub>2</sub>/MeOH gave **10** as an orange powder (252 mg, 4.9%). <sup>1</sup>H NMR (600 MHz, CDCl<sub>3</sub>):  $\delta$  = 8.19 (s, 3H; *meso*-Ar-*o*-H), 8.13 (s, 6H;  $\beta$ -H), 7.99 (d, *J* = 8.1 Hz, 3H; *meso*-Ar-*o*-H), 7.78 (d, *J* = 7.8 Hz, 3H; *meso*-Ar-*p*-H), 7.58 (t, *J* = 7.8 Hz, 3H; *meso*-Ar-*m*-H), 0.81 ppm (s, 3H; axial-OMe); <sup>11</sup>B NMR (193 MHz, CDCl<sub>3</sub>):  $\delta$  = -15.3 ppm (s, 1B); <sup>13</sup>C NMR (150 MHz, CDCl<sub>3</sub>):  $\delta$  = 141.3, 139.2, 135.9, 131.9, 131.2, 130.3, 122.9, 122.5, 119.3, 46.9 ppm (axial-OMe); UV/Vis (in CH<sub>2</sub>Cl<sub>2</sub>):  $\lambda$  ( $\epsilon$ ) = 373 (158 000), 460 nm (13 000 M<sup>-1</sup> cm<sup>-1</sup>); fluorescence (in CH<sub>2</sub>Cl<sub>2</sub>,  $\lambda_{\text{ex}}$  = 373 nm):  $\lambda_{\text{max}}$  = 517 nm,  $\Phi_{\text{F}}$  = 0.139; HR-ESIMS-TOF (positive mode): *m/z* calcd for C<sub>34</sub>H<sub>21</sub>N<sub>3</sub>B<sub>1</sub>Br<sub>3</sub>ONa: 759.9207 [M+Na]<sup>+</sup>; found: 759.9213.

**Methoxo(5,10,15-tri(3-benzamidophenyl)subporphyrinato)boron(III) (11):** Subporphyrin **10** (140 mg, 190  $\mu$ mol), benzamide (83 mg, 84  $\mu$ mol), [Pd<sub>2</sub>(dba)<sub>3</sub>] (4.9 mg, 5.3  $\mu$ mol), Xantphos (9.2 mg, 15.9  $\mu$ mol), Cs<sub>2</sub>CO<sub>3</sub> (260 mg, 800  $\mu$ mol), and degassed 1,4-dioxane (6 mL) were added to a 20 mL Schlenk tube under an N<sub>2</sub> atmosphere. The resulting mixture was degassed through three freeze-thaw cycles and then heated to 90 °C for 1 day. After cooling the solution the reaction mixture was passed through a short Celite pad and the solvent was evaporated. The crude product obtained was purified by GPC column chromatography (4 × 90 cm) and the axial ligand of the separated product was completely converted to the methoxo form by several dissolve-evaporate cycles in a mixture of

CH<sub>2</sub>Cl<sub>2</sub>/MeOH (1:1). Recrystallization of the residue from CH<sub>2</sub>Cl<sub>2</sub>/hexane gave subporphyrin **11** (133 mg, 82%). <sup>1</sup>H NMR (600 MHz, [D<sub>6</sub>]DMSO): δ = 10.63 (s, 3H; NH), 8.62 (s, 3H; *meso*-Ar-*o*-H), 8.37 (s, 6H; β-H), 8.12 (d, *J* = 8.2 Hz, 3H; *meso*-Ar-*o* or *p*-H), 8.04 (d, *J* = 7.4 Hz, 6H; Ph-*o*-H), 7.09 (d, *J* = 8.2 Hz, 3H; *meso*-Ar-*o* or *p*-H), 7.78 (t, *J* = 7.8 Hz, 3H; *meso*-Ar-*m*-H), 7.62 (t, *J* = 7.4 Hz, 3H; Ph-*p*-H), 7.56 (t, *J* = 7.3 Hz, 6H; Ph-*m*-H), 0.63 ppm (s, 3H; axial-OMe); <sup>11</sup>B NMR (193 MHz, CDCl<sub>3</sub>): δ = -15.5 ppm (brs, 1B); <sup>13</sup>C NMR (150 MHz, CDCl<sub>3</sub>): δ = 140.8, 138.8, 137.7, 134.6, 131.6, 129.2, 128.3, 127.3, 125.1, 123.3, 122.4, 120.1, 119.9, 46.6 ppm (axial-OMe); UV/Vis (in CH<sub>2</sub>Cl<sub>2</sub>): λ (ε) = 376 (164000), 462 nm (12000 M<sup>-1</sup> cm<sup>-1</sup>); fluorescence (in CH<sub>2</sub>Cl<sub>2</sub>, λ<sub>ex</sub> = 373 nm); λ<sub>max</sub> = 520 nm, Φ<sub>F</sub> = 0.178; HR-ESIMS-TOF (positive mode): *m/z* calcd for C<sub>53</sub>H<sub>39</sub>N<sub>6</sub>B<sub>1</sub>O<sub>4</sub>Na: 881.3027 [M+Na]<sup>+</sup>; found: 881.3022.

#### Methoxo(5,10,15-tri(3-aminophenyl)subporphyrinato)boron(III) (**8**)

**Reduction of nitro groups:** Subporphyrin **9** (10–50 mg) was dissolved in a minimal amount of chloroform, the solution was diluted with ethanol (15 mL) and 1 M aqueous HCl (15 mL) and SnCl<sub>2</sub>·2H<sub>2</sub>O (20 equiv) were added. The resulting mixture was vigorously stirred at 70 °C for 7 h. (The reaction was monitored by TLC. In case the reaction was sluggish, another 5–10 mL of 1 M aqueous HCl was added to the solution.) After cooling, 1 M aqueous NaOH was added to make the solution basic and the product was repeatedly extracted with CH<sub>2</sub>Cl<sub>2</sub> until the aqueous layer became colorless. The combined organic layer was washed with brine, dried over anhydrous Na<sub>2</sub>SO<sub>4</sub>, and the solvent was evaporated. The solid obtained was dissolved in methanol (ca. 20 mL) and the solution was heated at reflux for 30 min. After evaporating the solvent, the axially methoxo-coordinated product was recrystallized from CH<sub>2</sub>Cl<sub>2</sub>/hexane to give subporphyrin **8** quantitatively as an orange solid.

**Hydrolysis of amido groups:** Subporphyrin **11** (133 mg, 155 μmol) and NaOH (5.0 g) were dissolved in a mixture of EtOH (30 mL)/THF (3 mL)/water (10 mL). The resulting solution was heated at reflux overnight. After cooling the system, dilute hydrochloric acid (≈10%) was added to make the solution weakly basic. The product was extracted with CH<sub>2</sub>Cl<sub>2</sub> until the colored aqueous layer became colorless. The combined organic layer was washed with brine, dried over Na<sub>2</sub>SO<sub>4</sub>, and the solvent was evaporated. The axial ligand of the crude product was converted into the methoxo form through three dissolve–evaporate cycles in a mixture of CH<sub>2</sub>Cl<sub>2</sub>/MeOH (1:1). Finally, the crude product was recrystallized from CH<sub>2</sub>Cl<sub>2</sub>/hexane to give **8** (92 mg, 92%). <sup>1</sup>H NMR (600 MHz, CDCl<sub>3</sub>): δ = 8.13 (s, 6H; β-H), 7.45 (t, *J* = 7.6 Hz, 3H; *meso*-Ar-*m*-H), 7.41 (s, 3H; *meso*-Ar-*o*-H), 7.40 (d, *J* = 6.4 Hz, 3H; *meso*-Ar-*o*-H), 6.92 (d, *J* = 8.7 Hz, 3H; *meso*-Ar-*p*-H), 3.92 (brs, 6H; NH<sub>2</sub>), 0.81 ppm (s, 3H; axial-OMe); <sup>11</sup>B NMR (193 MHz, CDCl<sub>3</sub>): δ = -15.3 ppm (s, 1B); <sup>13</sup>C NMR (150 MHz, CDCl<sub>3</sub>): δ = 146.6, 140.9, 138.4, 129.5, 123.9, 122.2, 120.7, 120.0, 114.6, 46.8 ppm (axial-OMe); UV/Vis (in CH<sub>2</sub>Cl<sub>2</sub>): λ (ε) = 377 (170000), 489 nm (12000 M<sup>-1</sup> cm<sup>-1</sup>); fluorescence (in CH<sub>2</sub>Cl<sub>2</sub>, λ<sub>ex</sub> = 377 nm); λ<sub>max</sub> = 522 nm, Φ<sub>F</sub> = 0.09; HR-ESIMS-TOF (positive mode): *m/z* calcd for C<sub>33</sub>H<sub>24</sub>N<sub>6</sub>B<sub>1</sub>: 515.2156 [M-OMe]<sup>+</sup>; found: 515.2159.

**General procedure for preparing capped subporphyrins:** Trifluoroacetic acid (10 μL) and a tripodal aldehyde (1.0 equiv, 27.5 μmol) were added to a solution of subporphyrin **8** (15.0 mg, 27.5 μmol) in a mixture of CH<sub>2</sub>Cl<sub>2</sub> (360 mL) and *i*PrOH (90 mL) and the solution was stirred at room temperature for 1 day. After the addition of NaBH<sub>3</sub>CN (150 mg), the solution was stirred additional 1 day. The resulting solution was concentrated to ca. 20 mL by evaporation and then poured into water (50 mL). The product was extracted with CH<sub>2</sub>Cl<sub>2</sub> and the organic layer was washed with water, dried with Na<sub>2</sub>SO<sub>4</sub>, and the solvent was evaporated to dryness. The crude product was purified by gravity GPC column chromatography (4 × 90 cm, eluent: THF). The axial ligand of the obtained product was completely converted into the methoxo form through dissolve–evaporate cycles in a mixture of CH<sub>2</sub>Cl<sub>2</sub>/MeOH. Recrystallization from CH<sub>2</sub>Cl<sub>2</sub>/MeOH (for **12**, **13**, **14**, and **16**) or CH<sub>2</sub>Cl<sub>2</sub>/hexane (for **15**) gave the corresponding capped subporphyrin as an orange powder.

**Capped subporphyrin 12:** Yield: 80%; <sup>1</sup>H NMR (600 MHz, CDCl<sub>3</sub> at 25 °C): δ = 7.66 (d, *J* = 7.3 Hz, 3H; H<sup>b</sup>), 7.62 (d, *J* = 6.8 Hz, 3H; H<sup>e</sup>), 7.52 (t, *J* = 7.6 Hz, 3H; H<sup>c</sup>), 7.52 (s, 6H; β-H), 7.33 (t, *J* = 7.3 Hz, 3H; H<sup>d</sup>), 7.14 (s, 3H; H<sup>e</sup>), 7.11 (t, *J* = 6.9 Hz, 3H; H<sup>b</sup>), 6.98 (d, *J* = 8.2 Hz, 3H; H<sup>d</sup>), 6.80 (d, *J* = 8.3 Hz, 3H; H<sup>f</sup>), 5.77 (s, 3H; cap-H<sup>a</sup>), 4.95 (brt, 3H; NH), 4.43 (d,

*J* = 5.5 Hz, 6H; benzyl-H<sup>f</sup>), 3.90 (s, 6H; benzyl-H<sup>k</sup>), 0.56 ppm (s, 3H; axial-OMe); <sup>11</sup>B NMR (193 MHz, CDCl<sub>3</sub>): δ = -15.9 ppm (s, 1B); HR-ESIMS-TOF (positive mode): *m/z* calcd for C<sub>63</sub>H<sub>48</sub>N<sub>6</sub>B<sub>1</sub>O<sub>3</sub>: 947.3886 [M-OMe]<sup>+</sup>; found: 947.3884; UV/Vis (in CH<sub>2</sub>Cl<sub>2</sub>): λ (ε) 377 (144000), 461 (160000), 487 nm (11000 M<sup>-1</sup> cm<sup>-1</sup>); fluorescence (in CH<sub>2</sub>Cl<sub>2</sub>, λ<sub>ex</sub> = 377 nm); λ<sub>max</sub> = 507 nm, Φ<sub>F</sub> = 0.132.

**Capped subporphyrin 13:** Yield: 59%; <sup>1</sup>H NMR (600 MHz, [D<sub>6</sub>]DMSO at 25 °C): δ = 7.75 (d, *J* = 7.7 Hz, 3H; H<sup>e</sup> or H<sup>f</sup>), 7.66–7.62 (t, t, and d, 9H; H<sup>b</sup>, H<sup>i</sup>, and H<sup>e</sup> or H<sup>f</sup>), 7.50 (t, *J* = 7.8 Hz, 3H; H<sup>c</sup>), 7.19 (d, *J* = 7.3 Hz, 3H; H<sup>b</sup>), 7.17 (brs, 3H; β-H), 7.13 (d and brt, 6H; H<sup>d</sup> and NH), 6.75 (s, 3H; H<sup>e</sup>), 6.56 (s, 3H; cap-H<sup>a</sup>), 6.00 (brs, 3H; β-H), 5.48 (d, *J*<sub>gem</sub> = 10.1 Hz, 3H; benzyl-H<sup>k</sup>), 5.03 (d, *J*<sub>gem</sub> = 10.1 Hz, 3H; benzyl-H<sup>k</sup>), 4.73 (brd, 3H; benzyl-H<sup>f</sup>), 4.70 (brd, 3H; benzyl-H<sup>f</sup>), -0.03 ppm (s, 3H; axial-OMe); <sup>1</sup>H NMR (600 MHz, [D<sub>6</sub>]DMSO at 120 °C): δ = 7.79 (d, *J* = 7.4 Hz, 3H; H<sup>e</sup> or H<sup>f</sup>), 7.65 (d, *J* = 7.4 Hz, 3H; H<sup>e</sup> or H<sup>f</sup>), 7.62 (t, *J* = 7.3 Hz, 3H; H<sup>b</sup> or H<sup>i</sup>), 7.58 (t, *J* = 7.3 Hz, 3H; H<sup>b</sup> or H<sup>i</sup>), 7.50 (t, *J* = 7.3 Hz, 3H; H<sup>c</sup>), 7.24 (d, *J* = 7.3 Hz, 3H; H<sup>b</sup>), 7.14 (d, *J* = 8.2 Hz, 3H; H<sup>d</sup>), 6.84 (s, 3H; H<sup>e</sup>), 6.74 (brt, 3H; NH), 6.71 (brs, 6H; β-H), 6.67 (s, 3H; cap-H<sup>a</sup>), 5.28 (s, 6H; benzyl-H<sup>k</sup>), 4.76 (d, *J* = 5.5 Hz, 6H; benzyl-H<sup>f</sup>), 0.08 ppm (s, 3H; axial-OMe); UV/Vis (in CH<sub>2</sub>Cl<sub>2</sub> at 25 °C): λ (ε) 387 (136000), 471 (130000), 497 nm (17000 M<sup>-1</sup> cm<sup>-1</sup>); fluorescence (in CH<sub>2</sub>Cl<sub>2</sub>, λ<sub>ex</sub> = 387 nm); λ<sub>max</sub> = 515 nm, Φ<sub>F</sub> = 0.166; HR-ESIMS-TOF (positive mode): *m/z* calcd for C<sub>66</sub>H<sub>48</sub>N<sub>6</sub>B<sub>1</sub>O<sub>6</sub> and C<sub>67</sub>H<sub>51</sub>N<sub>6</sub>B<sub>1</sub>O<sub>6</sub>Na: 1031.3733 [M-OMe]<sup>+</sup>, 1085.3810 [M+Na]<sup>+</sup>; found: 1031.3736, 1085.3785.

**Capped subporphyrin 14:** Yield: 58%; <sup>1</sup>H NMR (600 MHz, CDCl<sub>3</sub> at 25 °C): δ = 7.78 (s, 6H; β-H), 7.77 (d, *J* = 7.3 Hz, 3H; H<sup>b</sup>), 7.55 (d, *J* = 7.4 Hz, 3H; H<sup>e</sup>), 7.53 (t, *J* = 7.4 Hz, 3H; H<sup>c</sup>), 7.28 (d, *J* = 7.4 Hz, 3H; H<sup>f</sup>), 7.10 (t, *J* = 7.4 Hz, 3H; H<sup>b</sup>), 6.93 (d, *J* = 8.1 Hz, 3H; H<sup>d</sup>), 6.76 (d, *J* = 8.4 Hz, 3H; H<sup>i</sup>), 6.64 (s, 3H; H<sup>e</sup>), 5.54 (s, 3H; cap-H<sup>a</sup>), 4.23 (brs, 6H; benzyl-H<sup>k</sup>), 4.20 (brs, 3H; NH), 3.99 (brt, 6H; ethylene), 3.72 (brt, 6H; ethylene), 0.75 ppm (s, 3H; axial-OMe); <sup>11</sup>B NMR (193 MHz, CDCl<sub>3</sub>): δ = -15.3 ppm (s, 1B); UV/Vis (in CH<sub>2</sub>Cl<sub>2</sub>): λ (ε) = 377 (132000), 461 nm (18000 M<sup>-1</sup> cm<sup>-1</sup>); fluorescence (in CH<sub>2</sub>Cl<sub>2</sub>, λ<sub>ex</sub> = 377 nm); λ<sub>max</sub> = 515 nm, Φ<sub>F</sub> = 0.133; HR-ESIMS-TOF (positive mode) *m/z* calcd for C<sub>66</sub>H<sub>54</sub>N<sub>6</sub>B<sub>1</sub>O<sub>6</sub>: 1037.4203 [M-OMe]<sup>+</sup>; found: 1037.4205.

**Capped subporphyrin 15:** Yield: 85%; <sup>1</sup>H NMR (600 MHz, CDCl<sub>3</sub> at 25 °C): δ = 7.64 (d, *J* = 7.3 Hz, 3H; H<sup>b</sup>), 7.60 (d, *J* = 7.6 Hz, 3H; H<sup>e</sup>), 7.53 (t, *J* = 8.3 Hz, 3H; H<sup>c</sup>), 7.36 (t, *J* = 6.8 Hz, 3H; H<sup>f</sup>), 7.28 (s, 6H; β-H), 7.20 (t, *J* = 7.3 Hz, 3H; H<sup>b</sup>), 7.00 (d, *J* = 8.3 Hz, 3H; H<sup>d</sup>), 6.83 (d, *J* = 7.8 Hz, 3H; H<sup>f</sup>), 6.54 (s, 3H; H<sup>e</sup>), 5.51 (s, 3H; cap-H<sup>a</sup>) 4.53 (brs, 3H; NH), 4.31 (brs, 6H; benzyl-H<sup>k</sup>), 3.93 (t, *J* = 5.0 Hz, 6H; -O-CH<sub>2</sub>-CH<sub>2</sub>-), 3.66 (t, *J* = 5.0 Hz, 6H; -O-CH<sub>2</sub>-CH<sub>2</sub>-), 1.99 (quintet, *J* = 5.0 Hz, 6H; -O-CH<sub>2</sub>-CH<sub>2</sub>-), 0.57 ppm (s, 3H; axial-OMe); <sup>11</sup>B NMR (193 MHz, CDCl<sub>3</sub>): δ = -15.8 ppm (s, 1B); UV/Vis (in CH<sub>2</sub>Cl<sub>2</sub>): λ (ε) = 382 (124000), 467 (130000), 493 nm (14000 M<sup>-1</sup> cm<sup>-1</sup>); fluorescence (in CH<sub>2</sub>Cl<sub>2</sub>, λ<sub>ex</sub> = 382 nm); λ<sub>max</sub> = 517 nm, Φ<sub>F</sub> = 0.156; HR-ESIMS-TOF (positive mode): *m/z* calcd for C<sub>69</sub>H<sub>60</sub>N<sub>6</sub>B<sub>1</sub>O<sub>6</sub>: 1079.4673 [M-OMe]<sup>+</sup>; found: 1079.4680.

**Capped subporphyrin 16:** Yield: 70%; <sup>1</sup>H NMR (600 MHz, CDCl<sub>3</sub> at 25 °C): δ = 8.40 (s, 3H; cap-H<sup>a</sup>), 7.63 (d, *J* = 7.3 Hz, 3H; H<sup>b</sup>), 7.56 (d, *J* = 7.8 Hz, 3H; H<sup>e</sup>), 7.53 (t, *J* = 7.3 Hz, 3H; H<sup>c</sup>), 7.38 (t, *J* = 6.8 Hz, 3H; H<sup>f</sup>), 7.27 (s, 6H; β-H), 7.18 (t, *J* = 7.4 Hz, 3H; H<sup>b</sup>), 6.99 (d, *J* = 7.3 Hz, 3H; H<sup>d</sup>), 6.82 (d, *J* = 7.8 Hz, 3H; H<sup>f</sup>), 6.48 (s, 3H; H<sup>e</sup>), 4.54 (brs, 9H; NH and -OCH<sub>2</sub>-), 4.31 (brd, 6H; benzyl-H<sup>k</sup>), 4.08 (brs, 6H; -OCH<sub>2</sub>-), 0.56 ppm (s, 3H; axial-OMe); <sup>11</sup>B NMR (193 MHz, CDCl<sub>3</sub>): δ = -15.8 ppm (s, 1B); UV/Vis (in CH<sub>2</sub>Cl<sub>2</sub>) λ (ε) 380 (108000), 466 (110000), 492 nm (12000 M<sup>-1</sup> cm<sup>-1</sup>); fluorescence (in CH<sub>2</sub>Cl<sub>2</sub>, λ<sub>ex</sub> = 380 nm); λ<sub>max</sub> = 534 nm, Φ<sub>F</sub> = 0.167; HR-ESIMS-TOF (positive mode): *m/z* calcd for C<sub>69</sub>H<sub>54</sub>N<sub>6</sub>B<sub>1</sub>O<sub>9</sub>: 1121.4051 [M-OMe]<sup>+</sup>; found: 1121.4045.

## Acknowledgements

This work was supported by a Grant-in-Aid (A) (No. 19205006) for Scientific Research from MEXT. Y.I. thanks the JSPS Research Fellowship for Younger Scientists.

- [1] Y. Inokuma, J. H. Kwon, T. K. Ahn, M.-C. Yoon, D. Kim, A. Osuka, *Angew. Chem.* **2006**, *118*, 975–978; *Angew. Chem. Int. Ed.* **2006**, *45*, 961–964.
- [2] a) R. Myśluborski, L. Latos-Grażyński, L. Sztrenberg, T. Lis, *Angew. Chem.* **2006**, *118*, 3752–3756; *Angew. Chem. Int. Ed.* **2006**, *45*, 3670–3674; b) E. A. Makarova, S. Shimizu, A. Matsuda, E. A. Luk'yanets, N. Kobayashi, *Chem. Commun.* **2008**, 2109–2111; c) Z.-L. Xue, Z. Shen, J. Mack, D. Kuzuhara, H. Yamada, T. Okujima, N. Ono, X.-Z. You, N. Kobayashi, *J. Am. Chem. Soc.* **2008**, *130*, 16478–16479.
- [3] a) T. Xu, R. Lu, X. Liu, P. Chen, X. Qiu, Y. Zhao, *Eur. J. Org. Chem.* **2008**, 1065–1071; b) Y. Inokuma, S. Hayashi, A. Osuka, *Chem. Lett.* **2009**, *38*, 206–207; c) Y. Inokuma, A. Osuka, *Dalton Trans.* **2008**, 2517–2526.
- [4] a) N. Kobayashi, Y. Takeuchi, A. Matsuda, *Angew. Chem.* **2007**, *119*, 772–774; *Angew. Chem. Int. Ed.* **2007**, *46*, 758–760; b) Y. Takeuchi, A. Matsuda, N. Kobayashi, *J. Am. Chem. Soc.* **2007**, *129*, 8271–8281; c) Y. Inokuma, Z. S. Yoon, D. Kim, A. Osuka, *J. Am. Chem. Soc.* **2007**, *129*, 4747–4761.
- [5] Y. Inokuma, S. Easwaramoorthi, S. Y. Jang, K. S. Kim, D. Kim, A. Osuka, *Angew. Chem.* **2008**, *120*, 4918–4921; *Angew. Chem. Int. Ed.* **2008**, *47*, 4840–4843.
- [6] Y. Inokuma, S. Easwaramoorthi, Z. S. Yoon, D. Kim, A. Osuka, *J. Am. Chem. Soc.* **2008**, *130*, 12234–12235.
- [7] Y. Inokuma, A. Osuka, *Org. Lett.* **2008**, *10*, 5561–5564.
- [8] E. Tsurumaki, S. Saito, K. S. Kim, J. M. Lim, Y. Inokuma, D. Kim, A. Osuka, *J. Am. Chem. Soc.* **2008**, *130*, 438–439.
- [9] E. Tsurumaki, Y. Inokuma, S. Easwaramoorthi, J. M. Lim, D. Kim, A. Osuka, *Chem. Eur. J.* **2009**, *15*, 237–247.
- [10] a) A. Meller, A. Ossko, *Monatsh. Chem.* **1972**, *103*, 150–155; b) C. G. Claessens, D. González-Rodríguez, T. Torres, *Chem. Rev.* **2002**, *102*, 835–853; c) T. Torres, *Angew. Chem.* **2006**, *118*, 2900–2903; *Angew. Chem. Int. Ed.* **2006**, *45*, 2834–2837.
- [11] Y. T. Wu, J. S. Siegel, *Chem. Rev.* **2006**, *106*, 4843.
- [12] a) H. Sakurai, T. Daiko, T. Hirao, *Science* **2003**, *301*, 1878; b) L. T. Scott, M. M. Hashemi, M. S. Bratcher, *J. Am. Chem. Soc.* **1992**, *114*, 1920–1921; c) A. Borchardt, A. Fuchicello, K. V. Kilway, K. K. Baldrige, J. S. Siegel, *J. Am. Chem. Soc.* **1992**, *114*, 1921–1923.
- [13] a) C. G. Claessens, T. Torres, *J. Am. Chem. Soc.* **2002**, *124*, 14522–14523; b) R. S. Iglesias, C. G. Claessens, T. Torres, G. M. A. Rahman, D. M. Guldi, *Chem. Commun.* **2005**, 2113–2115.
- [14] Y. Inokuma, A. Osuka, *Chem. Commun.* **2007**, 2938–2940.
- [15] a) W. Ma, K. M. Wilcoxon, J. W. Szweczyk, J. A. Ibers, *J. Org. Chem.* **1995**, *60*, 8081–8083; b) W. Ma, C. Sleboznick, J. A. Ibers, *J. Org. Chem.* **1993**, *58*, 6349–6353; c) A. Osuka, F. Kobayashi, K. Maruyama, *Bull. Chem. Soc. Jpn.* **1991**, *64*, 1213–1225; d) J. Almog, J. E. Baldwin, M. J. Crossley, J. F. Debernardis, R. L. Dyer, J. R. Huff, M. K. Peters, *Tetrahedron* **1981**, *37*, 3589–3601; e) R. P. Bonar-Law, J. K. M. Sanders, *J. Chem. Soc. Perkin Trans. 1* **1995**, 3085–3096; f) E. J. Rose, P. N. Venkatasubramanian, J. C. Swartz, R. D. Jones, F. Basolo, B. M. Hoffman, *Proc. Natl. Acad. Sci. USA* **1982**, *79*, 5742–5745; g) J. Almog, J. E. Baldwin, R. L. Dyer, M. Peters, *J. Am. Chem. Soc.* **1975**, *97*, 226–227; h) M. R. Johnson, W. K. Seok, J. A. Ibers, *J. Am. Chem. Soc.* **1991**, *113*, 3998–4000; i) R. P. Bonar-Law, J. K. M. Sanders, *J. Am. Chem. Soc.* **1995**, *117*, 259–271; j) H.-Y. Zhang, A. Blaskó, J.-Q. Yu, T. C. Bruce, *J. Am. Chem. Soc.* **1992**, *114*, 6621–6630; k) A. E. Rowan, P. P. M. Aarts, K. W. M. Koutstaal, *Chem. Commun.* **1998**, 611–612; l) M. J. Gunter, D. C. R. Hockless, M. R. Johnston, B. W. Skelton, A. H. White, *J. Am. Chem. Soc.* **1994**, *116*, 4810–4823.
- [16] a) J. A. Cowan, J. K. M. Sanders, *J. Chem. Soc. Perkin Trans. 1* **1985**, 2435–2437; b) D. Ricard, B. Andrioletti, M. L'Her, B. Boitrel, *Chem. Commun.* **1999**, 1523–1524; c) J. E. A. Webb, F. Maharaj, I. M. Blake, M. J. Crossley, *Synlett* **2008**, 2147–2149; d) B. Botta, P. Ricciardi, C. Galeffi, M. Botta, A. Tafi, R. Pogni, R. Iacovino, I. Garella, B. D. Blasio, G. D. Monache, *Org. Biomol. Chem.* **2003**, *1*, 3131–3137.
- [17] J. S. Lindsey, D. C. Mauzerall, *J. Am. Chem. Soc.* **1982**, *104*, 4498–4500.
- [18] J. Yin, S. L. Buchwald, *J. Am. Chem. Soc.* **2002**, *124*, 6043–6048.
- [19] a) P. D. W. Boyd, C. A. Reed, *Acc. Chem. Res.* **2005**, *38*, 235–242; b) T. Ishii, N. Aizawa, R. Kanehama, M. Yamashita, K. Sugiura, H. Miyasaka, *Coord. Chem. Rev.* **2002**, *226*, 113–124; c) K. Tashiro, T. Aida, J.-Y. Zheng, K. Kinbara, K. Saigo, S. Sakamoto, K. Yamaguchi, *J. Am. Chem. Soc.* **1999**, *121*, 9477–9478; d) M. Yanagisawa, K. Tashiro, M. Yamasaki, T. Aida, *J. Am. Chem. Soc.* **2007**, *129*, 11912–11913.
- [20] a) T. Kawase, H. Kurata, *Chem. Rev.* **2006**, *106*, 5250–5273; b) H. Sakurai, T. Daiko, H. Sakane, T. Amaya, T. Hirao, *J. Am. Chem. Soc.* **2005**, *127*, 11580–11581; c) R. Potz, M. Göldner, H. Hückstädt, U. Cornelissen, A. Tutaß, H. Homborg, *Z. Anorg. Allg. Chem.* **2000**, *626*, 588–596; d) M. S. Rodríguez-Morgade, C. G. Claessens, A. Medina, D. González-Rodríguez, E. Gutiérrez-Puebla, A. Monge, I. Alkorta, J. Elguero, T. Torres, *Chem. Eur. J.* **2008**, *14*, 1342–1350; e) B. W. Smith, M. Monthieux, D. E. Luzzi, *Nature* **1998**, *396*, 323–324; f) Y.-T. Wu, J. S. Siegel, *Chem. Rev.* **2006**, *106*, 4843–4867.
- [21] For subphthalocyanines,  $\pi(\text{bowl})$ – $\pi(\text{plane})$  interactions between a subphthalocyanine cation and an aromatic solvent have been reported, see: T. Kato, F. S. Tham, P. D. W. Boyd, C. A. Reed, *Heteroat. Chem.* **2006**, *17*, 209–216.
- [22] In the refinement of the crystal structure, the hydrogen atom of the axial B-OH group was generated at three equivalent positions with the same occupancy of 33.3% to preserve  $C_3$  molecular symmetry.
- [23] F. A. Samatey, K. Imada, S. Nagashima, F. Vonderviszt, T. Kumasa-ka, M. Yamamoto, K. Namba, *Nature* **2001**, *410*, 331–337.
- [24] a) S. Hiraoka, M. Shiro, M. Shionoya, *J. Am. Chem. Soc.* **2004**, *126*, 1214–1218; b) S. Hiraoka, E. Okuno, T. Tanaka, M. Shiro, M. Shionoya, *J. Am. Chem. Soc.* **2008**, *130*, 9089–9098.
- [25] Gaussian 03, Revision C.02, M. J. Frisch, G. W. Trucks, H. B. Schlegel, G. E. Scuseria, M. A. Robb, J. R. Cheeseman, J. A. Montgomery, Jr., T. Vreven, K. N. Kudin, J. C. Burant, J. M. Millam, S. S. Iyengar, J. Tomasi, V. Barone, B. Mennucci, M. Cossi, G. Scalmani, N. Rega, G. A. Petersson, H. Nakatsuji, M. Hada, M. Ehara, K. Toyota, R. Fukuda, J. Hasegawa, M. Ishida, T. Nakajima, Y. Honda, O. Kitao, H. Nakai, M. Klene, X. Li, J. E. Knox, H. P. Hratchian, J. B. Cross, V. Bakken, C. Adamo, J. Jaramillo, R. Gomperts, R. E. Stratmann, O. Yazyev, A. J. Austin, R. Cammi, C. Pomelli, J. W. Ochterski, P. Y. Ayala, K. Morokuma, G. A. Voth, P. Salvador, J. J. Dannenberg, V. G. Zakrzewski, S. Dapprich, A. D. Daniels, M. C. Strain, O. Farkas, D. K. Malick, A. D. Rabuck, K. Raghavachari, J. B. Foresman, J. V. Ortiz, Q. Cui, A. G. Baboul, S. Clifford, J. Cioslowski, B. B. Stefanov, G. Liu, A. Liashenko, P. Piskorz, I. Komaromi, R. L. Martin, D. J. Fox, T. Keith, M. A. Al-Laham, C. Y. Peng, A. Nanayakkara, M. Challacombe, P. M. W. Gill, B. Johnson, W. Chen, M. W. Wong, C. Gonzalez, J. A. Pople, Gaussian, Inc., Wallingford CT, **2004**.
- [26] TD-DFT calculations were also performed on the optimized structure of **13** at the B3LYP/6-31Gd level, which showed forbidden transition natures for the electronic transitions from HOMO–1 or HOMO to LUMO or LUMO+1 (see also the Supporting Information).
- [27] N. E. Kagan, D. Mauzerall, R. B. Merrifield, *J. Am. Chem. Soc.* **1977**, *99*, 5484–5486.

Received: April 3, 2009  
Published online: June 5, 2009